

Interplay between geometry and temperature for inclined Casimir plates

Alexej Weber¹ and Holger Gies²

¹*Institut für Theoretische Physik, Universität Heidelberg, Philosophenweg 16, D-69120 Heidelberg, Germany*

²*Theoretisch-Physikalisches Institut, Friedrich-Schiller-Universität Jena, Max-Wien-Platz 1, D-07743 Jena, Germany*
E-mail: a.weber@thphys.uni-heidelberg.de, holger.gies@uni-jena.de

We provide further evidence for the nontrivial interplay between geometry and temperature in the Casimir effect. We investigate the temperature dependence of the Casimir force between an inclined semi-infinite plate above an infinite plate in D dimensions using the worldline formalism. Whereas the high-temperature behavior is always found to be linear in T in accordance with dimensional-reduction arguments, different power-law behaviors at small temperatures emerge. Unlike the case of infinite parallel plates, which shows the well-known T^D behavior of the force, we find a T^{D-1} behavior for inclined plates, and a $\sim T^{D-0.3}$ behavior for the edge effect in the limit where the plates become parallel. The strongest temperature dependence $\sim T^{D-2}$ occurs for the Casimir torque of inclined plates. Numerical as well as analytical worldline results are presented.

I. INTRODUCTION

The Casimir effect [1] is not only a field witnessing rapid experimental as well as theoretical progress, it also continues to offer surprising new features. The Casimir effect derives its fascination from the fact that it originates from quantum fluctuations of the radiation field or of the charge distribution on the mesoscopic or macroscopic test bodies. Moreover, it inspires many branches of physics, ranging from mathematical to applied physics, see [2, 3] for reviews and [4] for experimental verifications.

A distinctive feature of Casimir forces between test bodies is the dependence on the geometry, i.e., the shape and orientation of these bodies. For a comparison between theory and a real Casimir experiment, a number of properties such as finite conductivity, surface roughness and finite temperature have to be taken into account in addition. Generically, these latter corrections do not factorize but take influence on one another. For instance, the interplay between dielectric material properties and finite temperature [5] is still a subject of intense theoretical investigations and has created a long-standing controversy [6, 7, 8, 9]. Also the role of electrostatic patch potentials has been suggested as a potentially problematic issue [10, 11], which has become a matter of severe debate [12, 13].

The present article is not meant to resolve these controversies. On the contrary, our work intends to draw attention to another highly nontrivial interplay which on the one hand needs to be accounted for when comparing theory and a real experiment and on the other hand is another characteristic feature of the Casimir effect: the interplay between geometry and temperature. As first conjectured by Jaffe and Scardicchio [14], the temperature dependence of the Casimir effect can be qualitatively different for different geometries, as both the pure Casimir effect as well as its thermal corrections arise from the underlying spectral properties of the fluctuations. First analytical as well as numerical evidence of this “geothermal” interplay in a perpendicular-plates configuration has been found in [15] using the worldline

formalism.

The physical reason for this interplay can be understood in simple terms: for the classical parallel-plate case, the nontrivial part of the fluctuation spectrum is given by the modes orthogonal to the plates. This relevant part of the spectrum has a gap of wave number $k_{\text{gap}} = \pi/a$, where a is the plate separation. For small temperatures $T \ll k_{\text{gap}}$, the higher-lying relevant modes can hardly be excited, such that their thermal contribution to the Casimir force remains suppressed: the resulting force law for the parallel-plates case scales like $(aT)^4$. This argument for a suppression of thermal contributions applies to all geometries with a gap in the relevant part of the spectrum (e.g. concentric cylinders or spheres, Casimir pistons, etc.). These geometries are called *closed*.¹

This reason for a suppression of thermal contributions is clearly absent for *open* geometries with a relevant gapless part of the spectrum. For these geometries, relevant modes of the spectrum can always be excited at any small temperature value. Therefore, a stronger thermal contribution $\sim (aT)^\alpha$ with $0 < \alpha < 4$ can be expected. As experimentally important configurations such as the sphere-plate or the cylinder-plate geometry belong to this class of open geometries, a potentially significant geothermal interplay may exist in the relevant parameter range $aT \sim 0.01 \dots 0.1$.

In the present work, we provide further evidence for the geometry-temperature interplay in the Casimir effect. For simplicity, we study the Casimir effect induced by a fluctuating real scalar field obeying Dirichlet boundary conditions (‘Dirichlet scalar’). As an illustrative example, we concentrate on an inclined-plates configuration; here, a semi-infinite plate is located above an infinite one, with an angle of inclination of $0 < \varphi \leq \pi/2$, see Fig. 1.

¹ Of course, parallel plates as well as concentric cylinders are not closed in the sense of compactness. Also, they have a gapless part of the spectrum along the symmetry axes. However, this part of the spectrum does not give rise to the Casimir force and hence is not a relevant part.

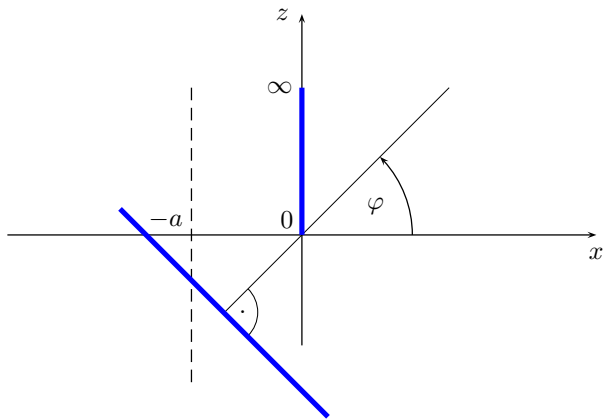


FIG. 1: Sketch of the inclined-plates configuration. The infinite plate (dashed line) is rotated in the x, z plane by an angle φ . As special cases, $\varphi = 0$ corresponds to the configuration of one semi-infinite plate parallel to an infinite plate (1si configuration), whereas $\varphi = \pi/2$ yields the perpendicular-plates configuration.

This configuration generalizes geometries which have first been proposed and studied in the context of Casimir edge effects [16]. Our results do not only generalize the findings of [15] which hold for $\varphi = \pi/2$. Most importantly, we identify regimes with fractional temperature dependences for certain geometries. Moreover, we work in $D = d + 1$ dimensional spacetime, yielding many analytical as well as numerical results for the Casimir force and energy as well as for the torque.

A reliable study of geothermal Casimir phenomena requires a method that is capable of dealing with very general Casimir geometries. For this, we use the worldline approach to the Casimir effect [17], which is based on a mapping of field-theoretic fluctuation averages onto quantum-mechanical path integrals [18, 19, 20]. For arbitrary backgrounds, this worldline integral representing the spacetime trajectories of the quantum fluctuations can straightforwardly be computed by Monte Carlo methods [21]. As the computational algorithm is generally independent of the background, i.e., the Casimir geometry in our case, Casimir problems can straightforwardly be tackled with this method. High-precision computations for Dirichlet-scalar fluctuations have been performed, e.g., for the sphere-plate and cylinder-plate case [22, 23, 24]. In the present work, we demonstrate that the worldline approach can also be used to obtain novel analytical results (see also [25] for an analytical worldline approximation technique).

In order to overcome standard approximative tools based, e.g., on the proximity-force theorem [26], a variety of new field-theoretical methods for Casimir phenomena have been developed in recent years, ranging from improved approximation methods [27, 28, 29] to exact methods mainly based on scattering theory [30, 31, 32, 33, 34, 35, 36, 37, 38] or a functional inte-

gral approach [39, 40, 41]. It will certainly be worthwhile to generalize these methods to finite temperature for a study of the geometry-temperature interplay.

In the remainder of this introduction, we summarize our most important results specializing to $3 + 1$ dimensional spacetime. In Sect. II, we briefly review the worldline approach to the Casimir effect. Sect. III is devoted to a study of the zero-temperature Casimir effect for the geometries under consideration. The finite-temperature case is described in Sect. IV. Our conclusions are summarized in Sect. V.

A. Summary of results in $D = 4$

Let us already summarize our most important results, specializing to $D = 4$ spacetime dimensions and concentrating on the Casimir interaction energy; the corresponding force can straightforwardly be derived by differentiation. At zero temperature, the classical Casimir energy of two parallel Dirichlet plates at a distance a reads

$$\frac{E_c^{\parallel}}{A} = -\frac{c_{\parallel} \hbar c}{a^3}, \quad c_{\parallel} = \frac{\pi^2}{1440} \approx 0.00685, \quad (1)$$

where A is the area of the plates. From now on, we use natural units, setting $\hbar c = 1$. The Casimir energy of inclined plates (i.p.) can be parameterized as

$$\frac{E_c^{i.p.,\varphi}}{L_y} = -\frac{c_{\varphi}}{\sin(\varphi) a^2}, \quad (2)$$

where the coefficient c_{φ} is shown in Fig. 4 as a function of φ . The extent of the inclined plate in y direction along the edge is L_y . At $\varphi = 0$, the energy per edge length (2) diverges and has to be replaced by

$$E_c^{1si} = E_c^{1si,\parallel} + E_c^{1si,edge} = -\frac{A^{1si} c_{\parallel}}{a^3} - \frac{L_y c_{edge}}{a^2}, \quad (3)$$

where $E_c^{1si,\parallel}$ is the Casimir Energy (1) with A^{1si} being the semi-infinite plate's area and $E_c^{1si,edge}$ the so-called edge energy. The numerical value of c_{edge} is about 0.0026 in agreement with [16].

The Casimir torque is obtained from Eq. (2) by $D_c^{i.p.,\varphi} = dE_c^{i.p.,\varphi}/d\varphi$. For $D = 4$, the torque $D_c^{i.p.,\varphi}$ as a function of φ is shown in Fig. 5. At $\varphi = 0$, the Casimir torque per unit length diverges as well but can be converted into finite torque per unit area. Remarkably, for $\varphi = 0$ the standard torque obtained from the Casimir energy of parallel plates (1) $D_c^{\parallel} = AL_z \pi^2/960a^4 \approx 0.0103AL_z/a^4$ is reduced by a repulsive contribution $\approx -0.003660L_y/a^2$ arising from the edge effect. We encounter a similar subleading repulsive torque effect at finite temperature.

Thermal fluctuations modify the Casimir energy, yielding the free energy

$$E_c(T) = E_c(0) + \Delta E_c(T), \quad (4)$$

where $\Delta E_c(T)$ is the temperature correction. For $(aT) \rightarrow 0$, the correction $\Delta E_c^{\parallel}(aT \rightarrow 0)$ to the well-known parallel-plates energy reads

$$\frac{\Delta E_c^{\parallel}(aT \rightarrow 0)}{A} = -\frac{\zeta(3)T^3}{4\pi} + \frac{\pi^2 a T^4}{90}, \quad (5)$$

which is $\approx -0.0957T^3 + 0.110aT^4$. Note that only the T^4 term contributes to the force as the first term vanishes upon differentiation.

For $(aT) \rightarrow 0$, our result for the thermal correction $\Delta E_c^{i.p.,\varphi}(T)$ to the inclined-plates energy reads

$$\frac{\Delta E_c^{i.p.,\varphi}(aT \rightarrow 0)}{L_y} = -\frac{c_{\varphi,T_0}T^2}{24 \sin(\varphi)} + \frac{\zeta(3)aT^3}{4\pi \sin(\varphi)}, \quad (6)$$

where c_{φ,T_0} is shown in Fig. 9 as a function of φ . The second term which is a purely analytical result is the generalization of a result for perpendicular plates, $\varphi = \pi/2$, found in [15]; numerically, this term evaluates to $\approx 0.0957aT^3/\sin(\varphi)$.

Again, Eq. (6) denotes an energy per edge length and diverges as $\varphi \rightarrow 0$. It has to be replaced by the formula for the energy of a semi-infinite plate above a parallel one, $E_c^{1si}(T) = E_c^{1si,edge}(T) + E_c^{1si,\parallel}(T)$. The thermal part of $E_c^{1si,\parallel}(T)$ is as in (5), where A is the area of the semi-infinite plate. The leading thermal correction to the edge effect $\Delta E_c^{1si,edge}(T)$ reads

$$\frac{\Delta E_c^{1si,edge}(T)}{L_y} = -\frac{c_{\varphi,T_0}T^2}{24} + 0.063a^{1.74}T^{3.74}, \quad (7)$$

For $(aT) \rightarrow \infty$, all thermal Casimir energies increase linearly in T due to dimensional reduction. For instance, the Casimir energy $E_c^{\parallel}(T)$ for parallel plates becomes

$$E_c^{\parallel}(aT \rightarrow \infty) = -\frac{A\zeta(3)T}{8\pi a^2}, \quad (8)$$

which is $\approx -0.0478AT/a^2$. Note that $E_c^{\parallel}(aT \rightarrow \infty)$ is independent of $\hbar c$ as the dimensional analysis easily shows. The energy at large (aT) can therefore be interpreted as a classical effect.

The same holds for the large (aT) behavior of the inclined-plates case as well as for semi-infinite plates. For inclined plates, we get

$$E_c^{i.p.,\varphi}(aT \rightarrow \infty) = -\frac{L_y \sqrt{\pi} c_{\varphi,T_{\infty}} T}{(4\pi)^2 a \sin(\varphi)}, \quad (9)$$

where $c_{\varphi,T_{\infty}}$ is shown in Fig. 9 as a function of φ .

The edge effect reads at large (aT)

$$E_c^{1si,edge}(aT \rightarrow \infty) = -\frac{0.016L_y T}{a}. \quad (10)$$

In main part of this article, these results will be derived in detail in D spacetime dimensions.

II. WORLDLINE APPROACH TO THE CASIMIR EFFECT

Let us briefly review the worldline approach to the Casimir effect for a massless Dirichlet scalar; for details, see [17, 24]. Consider a configuration Σ consisting of two rigid objects with surfaces Σ_1 and Σ_2 . The worldline representation of the Casimir interaction energy in $D = d+1$ dimensional spacetime reads

$$E_c = -\frac{1}{2(4\pi)^{D/2}} \int_0^{\infty} \frac{d\mathcal{T}}{\mathcal{T}^{1+D/2}} \int d^d x_{CM} \langle \Theta_{\Sigma}[\mathbf{x}(\tau)] \rangle. \quad (11)$$

Here, the generalized step functional obeys $\Theta_{\Sigma}[\mathbf{x}] = 1$ if a worldline $\mathbf{x}(\tau)$ intersects both surfaces $\Sigma = \Sigma_1 \cup \Sigma_2$, and is zero otherwise.

The expectation value in Eq. (11) is taken with respect to an ensemble of d -dimensional closed worldlines with a common center of mass \mathbf{x}_{CM} and a Gaussian velocity distribution,

$$\langle \dots \rangle = \frac{\int_{\mathbf{x}_{CM}} D\mathbf{x} \dots e^{-\frac{1}{4} \int_0^{\mathcal{T}} d\tau \dot{\mathbf{x}}^2(\tau)}}{\int_{\mathbf{x}_{CM}} D\mathbf{x} e^{-\frac{1}{4} \int_0^{\mathcal{T}} d\tau \dot{\mathbf{x}}^2(\tau)}}. \quad (12)$$

Here, we have already used the fact that the time component cancels out for static Casimir configurations at zero temperature. Eq. (11) has an intuitive interpretation: All worldlines intersecting both surfaces do not satisfy Dirichlet boundary conditions on both surfaces. They are removed from the ensemble of allowed fluctuations by the Θ functional and thus contribute to the negative Casimir interaction energy. In the process of the auxiliary \mathcal{T} integration, the proper-time parameter \mathcal{T} scales the extent of a worldline by a factor of $\sqrt{\mathcal{T}}$. Large \mathcal{T} correspond to long-wavelength or IR fluctuations, small \mathcal{T} to short-wavelength or UV fluctuations.

Introducing finite temperature $T = 1/\beta$ by the Matsubara formalism is equivalent to compactifying Euclidean time on the interval $[0, \beta]$. Now, the closed worldlines live on a cylindrical surface and can carry a winding number. The worldlines $\mathbf{x}^{(n)}(\tau)$ winding n times around the cylinder can be decomposed into a worldline $\tilde{\mathbf{x}}(\tau)$ with no winding number and a winding motion at constant speed,

$$x_i^{(n)}(\tau) = \tilde{x}_i(\tau) + \frac{n\beta\tau}{\mathcal{T}} \delta_{iD}, \quad (13)$$

where the D th component corresponds to Euclidean time. The Casimir energy (11) now becomes

$$E_c = -\frac{1}{2(4\pi)^{D/2}} \times \int_0^{\infty} \frac{d\mathcal{T}}{\mathcal{T}^{1+D/2}} \sum_{n=-\infty}^{\infty} e^{-\frac{n^2\beta^2}{4\mathcal{T}}} \int d^d x_{CM} \langle \Theta_{\Sigma}[\mathbf{x}(\tau)] \rangle. \quad (14)$$

The finite-temperature worldline formalism for static configurations thus boils down to a winding-number prefactor in front of the worldline expectation value together

with a sum over winding numbers:

$$\langle \dots \rangle \rightarrow \left(1 + 2 \sum_{n=1}^{\infty} e^{-\frac{n^2 \beta^2}{4\mathcal{T}}} \right) \langle \dots \rangle. \quad (15)$$

The winding-number sum is directly related to the standard Matsubara sum by a Poisson resummation,

$$\left(1 + 2 \sum_{n=1}^{\infty} e^{-\frac{n^2 \beta^2}{4\mathcal{T}}} \right) = \frac{\sqrt{4\pi\mathcal{T}}}{\beta} \sum_{n=-\infty}^{\infty} e^{-(\frac{2\pi n}{\beta})^2 \mathcal{T}}. \quad (16)$$

This is already sufficient to understand the high-temperature limit of generic Casimir configurations: at high temperatures $\beta \rightarrow 0$, only the zeroth Matsubara frequency survives as higher modes receive thermal masses of order $\sim 2\pi/\beta = 2\pi T$ and decouple. All remaining temperature dependence arises from the dimensional prefactor $1/\beta = T$, and the dependence on the Casimir geometry only enters the prefactor. The calculation of the latter is a dimensionally reduced problem in $D - 1$ dimensions. This is a general mechanism of *dimensional reduction* in high-temperature field theories. The linear high-temperature asymptotics is also clear from the fact that the Bose-Einstein distribution governing the distribution of bosonic thermal fluctuations increases as $\sim T$ in the high-temperature limit.

Finally, it is advantageous for numerical as well as analytical calculations to rescale the worldlines such that the velocity distribution becomes independent of \mathcal{T} ,

$$\gamma(t) := \frac{1}{\sqrt{\mathcal{T}}} \mathbf{x}(\mathcal{T}t) \rightarrow e^{-\frac{1}{4} \int_0^{\mathcal{T}} \dot{\mathbf{x}}^2 d\tau} = e^{-\frac{1}{4} \int_0^1 \dot{\gamma}^2 dt}, \quad (17)$$

where the dot always denotes a derivative with respect to the argument, e.g., $\dot{\gamma} = d\gamma(t)/dt$. In terms of these normalized worldlines γ and the center-of-mass coordinate \mathbf{x}_{CM} , the Θ function reads more explicitly

$$\Theta[\mathbf{x}] \equiv \Theta[\mathbf{x}_{\text{CM}} + \sqrt{\mathcal{T}}\gamma(t)]. \quad (18)$$

The involved worldline integrals can be evaluated also numerically by Monte Carlo methods in a straightforward manner. For this, the path integral over an operator \mathcal{O} is approximated by a sum over a finite ensemble of n_L loops,

$$\langle \mathcal{O}[\gamma] \rangle \rightarrow \frac{1}{n_L} \sum_{\ell=1}^{n_L} \mathcal{O}[\gamma_\ell], \quad (19)$$

where ℓ counts the worldlines in the ensemble. Each worldline $\gamma(t)$ is furthermore discretized by a finite set of N points per loop (ppl),

$$\gamma(t) \rightarrow \gamma_i = \gamma(t_i), \quad t_i = \frac{i}{N}, \quad i = 0, \dots, N, \quad (20)$$

where $\gamma_0 = \gamma_N$ are identified as the worldlines are closed. Various efficient ab initio algorithms for generating discretized worldlines with Gaussian velocity distribution have been developed, see, e.g., [17, 42].

With these comparatively simple prerequisites, we can now turn to an analysis of various non-trivial Casimir configurations for the Dirichlet scalar.

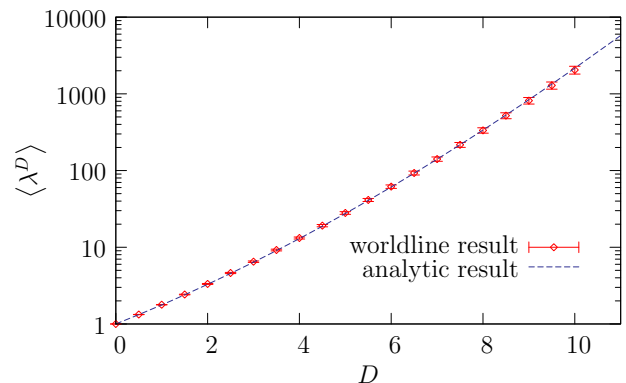


FIG. 2: D th moment of the maximum spatial extent λ of a worldline as a function of D . This geometric object (which is the same in any target dimension of the worldline) is related to the Casimir energy of the parallel-plates configuration in D spacetime dimensions by Eqs. (23) and 24. The plot compares the exact analytical result with the worldline numerical computation based on 1000 worldlines with 2×10^6 ppl (points per loop) each.

III. CASIMIR EFFECT AT ZERO TEMPERATURE

Let us first study parallel and inclined plates at zero temperature. The purpose of this section is on the one hand to review and generalize known results and on the other hand to exemplify how the Casimir effect can be understood in terms of simple geometric properties of the worldlines.

A. Parallel Plates

We start with Casimir's classic configuration of two infinitely extended parallel plates. Let the lower and upper plate lie in the $z = -a$ and $z = 0$ planes, respectively. In d space dimensions the surface area A of the plates is then $d - 1$ dimensional. The Θ functional for this configuration reads

$$\Theta_{\parallel} \left[z_{\text{CM}} + \sqrt{\mathcal{T}}\gamma_{z,\ell} \right] = \theta \left(\sqrt{\mathcal{T}}\gamma_{z_{\text{max},\ell}} + z_{\text{CM}} \right) \times \theta \left(-z_{\text{CM}} - \sqrt{\mathcal{T}}\gamma_{z_{\text{min},\ell}} - a \right), \quad (21)$$

where $\gamma_{z,\ell}$ is the z coordinate of the ℓ 'th worldline (measured with respect to the center of mass). The quantities $\gamma_{z_{\text{max},\ell}}$, $\gamma_{z_{\text{min},\ell}}$ denote the worldline's maximal and minimal extent in the z direction, respectively. The total maximal extent λ_ℓ of the ℓ 'th worldline then is $\lambda_\ell = \gamma_{z_{\text{max},\ell}} - \gamma_{z_{\text{min},\ell}}$. Now, we can do the integral in Eq. (11) and obtain the Casimir energy density (suppressing the index ℓ from now on)

$$\frac{E_{\parallel}^c}{A} = - \frac{\langle \lambda^D \rangle}{D(D-1)(4\pi)^{D/2} a^{D-1}}. \quad (22)$$

We observe that the D -dimensional parallel-plate Casimir energy is related to the D th cumulant of the extent of the worldlines [24]. This is a first example for a relation between Casimir energies and geometric properties of the worldlines. Instead of computing these cumulants directly, let us simply compare Eq. (22) with the well-known analytic result [43, 44].

$$\frac{E_c^{\parallel}}{A} = -\frac{\Gamma(D/2)\zeta(D)}{(4\pi)^{D/2} a^{D-1}}, \quad (23)$$

yielding

$$\langle \lambda^D \rangle = D(D-1)\Gamma(D/2)\zeta(D). \quad (24)$$

A comparison of the analytical result to a numerical evaluation of the cumulants is displayed in Fig. 2. Also, the Casimir force density can straightforwardly be obtained as the derivative of Eq. (22) with respect to a . Incidentally, the connection between Casimir energies and worldline properties also induces a relation between Casimir energies and questions in polymer physics, as first observed in [24].

B. Inclined plates

The inclined-plates (i.p.) configuration consists of a perfectly thin semi-infinite plate above an infinite plate at an angle φ , see Fig. 1. The semi-infinite plate has an edge with a $(d-2)$ dimensional length L_y . The infinite plate has a $(d-1)$ dimensional area A .² Let a be the minimal distance between the plates. In the following, we will omit the center-of-mass subscript CM. The Θ functional for this configuration reads

$$\begin{aligned} \Theta_{\text{i.p.},\varphi} = & \theta\left(-x \cos(\varphi) - z \sin(\varphi) - \sqrt{\mathcal{T}} \gamma_{x_{\min},\ell}(\varphi) - a\right) \\ & \times \theta\left(z + \sqrt{\mathcal{T}} \gamma_{z_{\max},\ell}\left(-\frac{x}{\sqrt{\mathcal{T}}}\right)\right) \\ & \times \theta\left(-x - \sqrt{\mathcal{T}} \gamma_{x_{\min},\ell}\right) \theta\left(x + \sqrt{\mathcal{T}} \gamma_{x_{\max},\ell}\right), \end{aligned} \quad (25)$$

where the first θ function ensures the intersection of the worldline with the infinite plate. The remaining three ones account for the intersection with the semi-infinite plate. In Eq. (25), we have used

$$\gamma_{x_{\min},\ell}(\varphi) \equiv \min_t (\gamma_{x,\ell}(t) \cos(\varphi) + \gamma_{z,\ell}(t) \sin(\varphi)), \quad (26)$$

where t parameterizes the worldline; i.e., in the discretized version, we have $t = 1 \dots N$ with N being the number of points per worldline loop (ppl). Trivially, $\gamma_{x_{\min},\ell}(0) = \gamma_{x_{\min},\ell}$ and $\gamma_{x_{\min},\ell}(\pi/2) = \gamma_{z_{\min},\ell}$ holds.

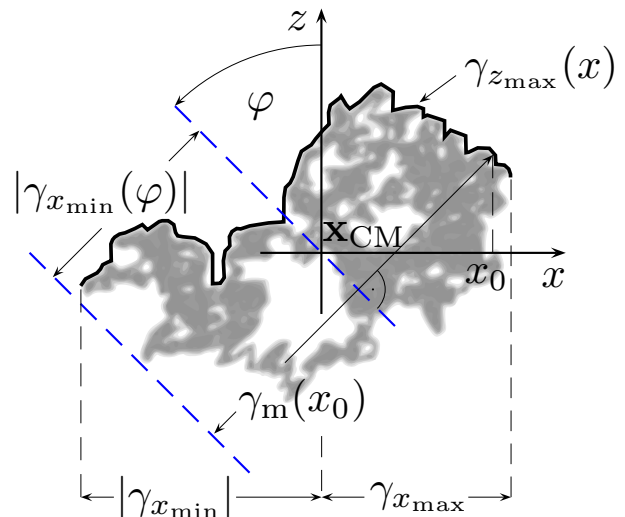


FIG. 3: All relevant information for the evaluation of the Casimir energy of the inclined plates, (28), is encoded in the function $\gamma_m(x)$, which has to be integrated from $\gamma_{x_{\min}}$ to $\gamma_{x_{\max}}$.

In other words, $\gamma_{x_{\min},\ell}(\varphi)$ measures the minimal extent of the worldline in the x direction of a coordinate system rotated by the angle φ . In Eq. (25), we also encounter $\gamma_{z_{\max},\ell}(x)$, denoting the x -dependent envelope of the worldline in positive z direction. All these geometric properties of a worldline are displayed in Fig. 3.

The $\Theta_{\text{i.p.},\varphi}$ functional in Eq. (25) generalizes the case of perpendicular plates (\perp) for $\varphi = \pi/2$ and the case of one semi-infinite plate parallel to a infinite one (1si) for $\varphi \rightarrow 0$; both edge configurations were studied in detail in [16, 45].

Let us define

$$\gamma_m(x) \equiv x \cos(\varphi) + \sin(\varphi) \gamma_{z_{\max}}(x) - \gamma_{x_{\min}}(\varphi). \quad (27)$$

Inserting $\Theta_{\text{i.p.},\varphi}$ for $\varphi \neq 0$ into Eq. (11) leads to the Casimir energy density of the inclined plates

$$\begin{aligned} \frac{E_c^{\text{i.p.},\varphi}}{L_y} = & -\frac{\csc(\varphi)}{(4\pi)^{D/2}(D-1)(D-2) a^{D-2}} \\ & \times \left\langle \int_{\gamma_{x_{\min}}}^{\gamma_{x_{\max}}} dx \gamma_m^{D-1}(x) \right\rangle. \end{aligned} \quad (28)$$

Equation (28) is shown as a function of φ in Fig. 4 for $D = 4$. For $\varphi = \pi/2$ and $D = 4$, we rediscover the perpendicular plates result [16, 45] as a special case. Incidentally, the integral in Eq. (28) can be done analytically for $\varphi = 0$ resulting in $\langle \lambda^D/D \rangle = (D-1)\Gamma(D/2)\zeta(D)$. Together with the φ -dependent prefactor, Eq. (28) diverges as $\varphi \rightarrow 0$ as it should. This is because Eq. (28) corresponds to the energy per unit *edge length*, whereas for $\varphi \rightarrow 0$ the Casimir energy becomes proportional to the *area* of the semi-infinite plate. We devote the whole next

² Of course, the labels “semi-infinite” and “infinite” imply that both L_y and A are considered in the limit $L_y, A \rightarrow \infty$.

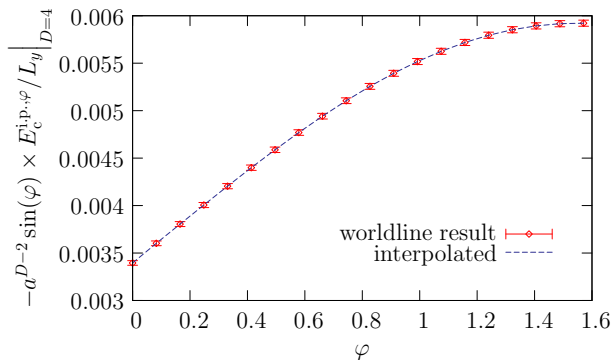


FIG. 4: Normalized Casimir energy per edge length $-\frac{E_c^{i.p.,\varphi}}{L_y} \times a^{D-2} \sin(\varphi)$ of the inclined-plates (i.p.) configuration in $D = 4$ versus the angle of inclination φ . For $\varphi = 0$, this function can be evaluated analytically, yielding $\pi^2/2880 \approx 3.427 \cdot 10^{-3}$. We have used 20000 worldlines with 10^6 ppl each.

section to analyzing how the limit $\varphi \rightarrow 0$ yielding the 1si configuration can be obtained.

C. Inclined plates, $\varphi \rightarrow 0$ limit

It is instructive to study the limit of a semi-infinite plate parallel to an infinite plate (1si), $\varphi \rightarrow 0$, as it involves a subtle limiting process. Recalling the general considerations of [16, 45] for the 1si case, the total Casimir interaction energy decomposes into

$$E_c^{1si} = E_c^{1si,\parallel} + E_c^{1si,edge}, \quad (29)$$

where $E_c^{1si,\parallel}/A$ is the usual Casimir energy per unit area of two parallel plates Eq. (23), with A being now the area of the semi infinite plate. The so called edge energy $E_c^{1si,edge}$ measures the contribution that arises solely due to the presence of the edge.

In the limit $\varphi \rightarrow 0$, this decomposition is naturally achieved by inserting $\Theta_{i.p.,\varphi=0}$ of Eq. (25) into Eq. (11) and performing the z integral first. This leads to

$$\frac{E_c^{1si,edge}}{L_y} = -\frac{1}{(4\pi)^{D/2}(D-2)a^{D-2}} \times \left\langle \int_{\gamma_{x_{\min}}}^{\gamma_{x_{\max}}} dx \gamma_{z_{\max}}(x)(x - \gamma_{x_{\min}})^{D-2} \right\rangle. \quad (30)$$

This representation can straightforwardly be computed numerically [16]. Of course, for truly infinite plates, the edge effect being proportional to the length of the edge is completely negligible in comparison with $E_c^{1si,\parallel}$, the latter being proportional to the area of the plates. However, dealing with finite plates, the edge effect contributes to the Casimir force, effectively increasing the plate's area [16].

Of course, the same result has to arise from the general inclined-plates formula Eq. (28) in the limit $\varphi \rightarrow 0$. However, this representation naively exhibits a divergence in this limit. To find the origin of the divergence, we decompose Eq. (28) into the parts corresponding to the edge effect $E_c^{edge,\varphi}$ and the semi-infinite-plates energy $E_c^{\parallel,\varphi}$, characterized by the integrals $\int_{-\gamma_{z_{\max}(x)}}^0 \dots dz$ and $\int_0^{L_z/2} \dots dz$, respectively. Here $L_z/2$ denotes the (infinite) length of the semi-infinite plate in z direction. The result for $E_c^{edge,\varphi}$ reads

$$E_c^{edge,\varphi} = -\frac{L_y}{(4\pi)^{D/2}(D-2)a^{D-2}} \times \left\langle \int_{\gamma_{x_{\min}}}^{\gamma_{x_{\max}}} \gamma_{z_{\max}}(x) \gamma_m^{D-2}(x) dx \right\rangle, \quad (31)$$

which becomes E_c^{edge} in Eq. (30) as $\varphi \rightarrow 0$; Eq. (31) is therefore valid for $\varphi = 0$.

On the other hand, if we naively expand the result for $E_c^{\parallel,\varphi}$ for small φ , we obtain

$$E_c^{\parallel,\varphi} \stackrel{?}{=} \frac{-\langle \lambda^D \rangle L_y}{(4\pi)^{D/2}(D-2)(D-1)Da^{D-2}\varphi} + O(\varphi), \quad (32)$$

which is only valid for $\varphi \neq 0$ and does not reproduce Eq. (22) in the limit $\varphi \rightarrow 0$. Instead of the energy per area, we have obtained the energy per length, which of course diverges in this limit. In order to rediscover the Casimir energy for the 1si configuration, the limits $\varphi \rightarrow 0$ and the implicit limit $L_z \rightarrow \infty$ have to be taken in the right order. In Eq. (32), the limit $L_z \rightarrow \infty$ has implicitly been performed first, which precisely leads to the divergence of the energy per edge length. Therefore, we need to first perform the limit $\varphi \rightarrow 0$ at finite L_z in order to obtain the desired energy per area. Starting from $E_c^{\parallel,\varphi}$ at small φ ,

$$E_c^{\parallel,\varphi \rightarrow 0} = -\frac{L_y}{2(4\pi)^{D/2}} \left\langle \int_0^\infty \frac{d\mathcal{T}}{\mathcal{T}^{(D+1)/2}} \int_0^{L_z/2} dz \times \int_{\gamma_{x_{\min}}}^{\gamma_{x_{\max}}} dx \theta \left(-a + \sqrt{\mathcal{T}}x - z\varphi - \sqrt{\mathcal{T}}\gamma_{x_{\min}} \right) \right\rangle, \quad (33)$$

we do the \mathcal{T} integral *first* and obtain

$$E_c^{\parallel,\varphi \rightarrow 0} = -\frac{L_y \langle \lambda^D \rangle (a^{2-D} - (a + L_z\varphi/2)^{2-D})}{(4\pi)^{D/2}(D-2)(D-1)D\varphi}. \quad (34)$$

For small $(L_z\varphi)$, i.e., finite L_z and $\varphi \rightarrow 0$, we can expand the last factor in φ ,

$$E_c^{\parallel,\varphi \rightarrow 0} \cong -\frac{L_y \langle \lambda^D \rangle}{(4\pi)^{D/2}(D-1)D} \times \left(\frac{1}{2}a^{1-D}L_z - \frac{1}{8}a^{-D}(D-1)L_z^2\varphi \right), \quad (35)$$

which for $\varphi \equiv 0$ corresponds exactly to the parallel-plates contribution $E_c^{1si,\parallel}$ in Eq. (22). From Eq. (34), we

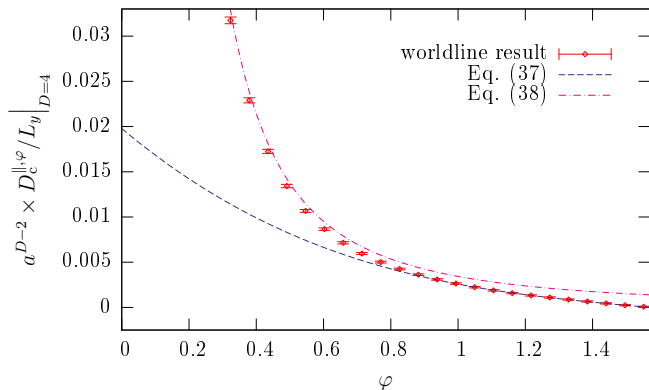


FIG. 5: Normalized Casimir torque per edge length $\frac{D_c^{\text{i.p.}, \varphi}}{L_y} \times a^{D-2}$ of the inclined-plates configuration in $D = 4$ and its expansion around $\varphi = \pi/2$ and $\varphi = 0$, respectively, versus the angle of inclination φ . We have used 10000 worldlines with 10^6 ppl each.

also observe that the other order of limits, taking first $L_z \rightarrow \infty$ while keeping φ finite, reproduces the divergent behavior of the energy per edge length in Eq. (32) (as long as $\text{Re}[D] > 2$). The proper order of limits is similarly important at finite temperature with the additional complication that another dimensionful parameter occurs.

D. Casimir torque of inclined plates

The Casimir torque $D_c^{\text{i.p.}, \varphi}$ referring to rotations of one of the plates about the edge axis can easily be obtained by taking the derivative of the Casimir energy (28), (or Eq. (34) for small φ), with respect to the angle of inclination:

$$D_c^{\text{i.p.}, \varphi} = \frac{dE_c^{\text{i.p.}, \varphi}}{d\varphi}. \quad (36)$$

For φ near $\pi/2$, we can even set $d\gamma_{x_{\min}}(\varphi)/d\varphi = 0$ before taking the average with respect to the loop ensemble, simplifying the calculations. This is, because the derivative $d\gamma_{x_{\min}}(\varphi)/d\varphi$ changes its sign for perpendicular plates $\varphi = \pi/2$ if the worldline is rotated by an angle π about the normal axis of the lower plate, see Fig. 1. Therefore, the sign correlates with the position of the minimum on the x axis of the lower plate. But the position x of the minimum $\gamma_{x_{\min}}(\varphi)$ does not correlate with the value of the integral in Eq. (28) leading to a mutual cancellation of terms involving $d\gamma_{x_{\min}}(\varphi)/d\varphi$.

For $\varphi < \pi/2$, we have to rotate the worldline about the normal axis of the inclined lower plate. Then, the correlation between the position of the minimum and the involved integrals does not vanish any more since the original and rotated worldline contribute differently to

the integral. In general, expressions containing derivatives of $\gamma_{x_{\min}}(\varphi)$ cannot be neglected even at $\varphi = \pi/2$. Since the worldlines are not smooth, the convergence of averages of such expressions will be very slow. This is the case when calculating the coefficients of an expansion of Eq. (36) near $\varphi = \pi/2$. Since the second derivative already appears in the first expansion coefficient, more confident values are obtained by a numerical fit to Eq. (36). There, only the first derivative is present. For $D = 4$, we obtain (see Fig. 5)

$$\frac{D_c^{\text{i.p.}, \varphi \rightarrow \pi/2} a^2}{L_y} \approx 0.00329 \left(\frac{\pi}{2} - \varphi\right) + 0.0038 \left(\frac{\pi}{2} - \varphi\right)^3. \quad (37)$$

This should be compared to the worldline average based on the expansion of Eq. (36) around $\pi/2$: the linear coefficient in Eq. (37) then yields 0.003 ± 0.0002 . If we neglect all derivatives of $\gamma_{x_{\min}}(\varphi)$ the worldline result reads 0.00285 ± 0.00003 . In all three cases 10000 worldlines with 10^6 ppl were used.

For $\varphi \rightarrow 0$, the Casimir torque diverges. The expansion about $\varphi = 0$ can easily be obtained analytically from (34)

$$D_c^{\text{i.p.}, \varphi \rightarrow 0} \simeq \frac{L_y \Gamma(D/2) \zeta(D)}{(4\pi)^{D/2} (D-2) a^{D-2} \varphi^2}, \quad (38)$$

where we have used Eq. (24). For $D = 4$, Eq. (38) yields $L_y \pi^2 / 2880 a^2 \varphi^2 \approx 0.00343 L_y / a^2 \varphi^2$, being excellent approximation to Eq. (36) for φ not too close to $\pi/2$.

The divergent Casimir torque per length can be converted into finite torque per unit area by means of Eq. (34). Note that Eq. (34) leads to the classical result for the torque,

$$D_c^{\parallel, \varphi \rightarrow 0} = \frac{A L_z \Gamma(D/2) \zeta(D) (D-1)}{2(4\pi)^{D/2} a^D}, \quad (39)$$

where A and L_z denote the semi-infinite plate's area and extent in z direction, respectively. For $D = 4$, Eq. (39) becomes $A L_z \pi^2 / 960 a^4 \approx 0.0103 A L_z / a^4$.

A new characteristic contribution emerges from the edge effect Eq. (31). Unlike the total inclined-plate Casimir energy $E_c^{\text{i.p.}, \varphi} = E_c^{\parallel, \varphi} + E_c^{\text{edge}, \varphi}$, the edge energy (31) decreases with the angle of inclination φ , see Fig. 6. This leads to a contribution which works against the standard torque (39). For $D = 4$, the correction to Eq. (39) emerging from the edge effect reads

$$D_c^{\text{edge}, \varphi \rightarrow 0} = -(0.003660 \pm 0.000038) \frac{L_y}{a^2}, \quad (40)$$

where we have used 10000 worldlines with 10^6 ppl each. The coefficient in Eq. (40) was calculated by expanding Eq. (31) around $\varphi = 0$. Equation (40) is shown in Fig. 6. We will see a similar subleading repulsive torque effect in the next section where we investigate finite-temperature contributions.

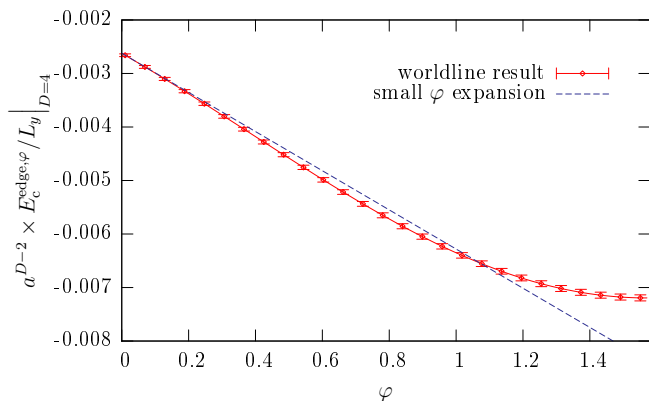


FIG. 6: Normalized edge energy per edge length $\frac{E_c^{\text{edge}, \varphi}}{L_y} \times a^{D-2}$ of the inclined-plates configuration in $D = 4$ and its expansion around $\varphi = 0$ versus the angle of inclination φ . We have used 10000 worldlines with 10^6 ppl each.

IV. FINITE TEMPERATURE

Decomposing the Casimir energy at finite temperature $T = 1/\beta$ into its zero-temperature part $E_c(0)$ and finite-temperature correction $\Delta E_c(T)$,

$$E_c(T) = E_c(0) + \Delta E_c(T), \quad (41)$$

is straightforward in the worldline picture by using the relation (15). The finite-temperature correction is purely driven by the worldlines with nonzero winding number. As the winding-number sum does not take direct influence on the worldline averaging, the complicated geometry-dependent part of the calculation remains the same for zero or finite temperature. This disentangles the technical complications arising from geometry on the one hand and temperature on the other hand in a convenient fashion. The same statement holds for the Casimir force $F_c(T) = F_c(0) + \Delta F_c(T)$.

A. Parallel plates

In order to demonstrate the simplicity of the worldline method, let us calculate the well-known thermal contribution to the Casimir effect for parallel plates. In the following, we use the dimensionless parameter

$$\xi \equiv aT, \quad (42)$$

which distinguishes between the high-temperature $\xi \gg 1$ and low-temperature $\xi \ll 1$ parameter region.

Evaluating the general worldline formula for the Casimir energy Eq. (14) using the parallel-plates Θ func-

tional of Eq. (21) results in ($D > 2$)

$$\begin{aligned} \frac{\Delta E_c^{\parallel}(\xi)}{E_c^{\parallel}(0)} &= \frac{\Gamma\left(\frac{D-1}{2}\right) \sqrt{\pi} \zeta(D-1) (2\xi)^{D-1}}{\Gamma(D/2) \zeta(D)} - (2\xi)^D \\ &+ \left\langle \sum_{n=1}^{\infty} \frac{\lambda^D}{\Gamma(D/2) \zeta(D)} \right. \\ &\times \left[E_{1-\frac{D}{2}} \left(\frac{\lambda^2 n^2}{4\xi^2} \right) - E_{\frac{3}{2}-\frac{D}{2}} \left(\frac{\lambda^2 n^2}{4\xi^2} \right) \right] \Bigg\rangle, \end{aligned} \quad (43)$$

where the exponential integral function $E_n(z)$ is given by

$$E_n(z) \equiv \int_1^{\infty} \frac{e^{-zt}}{t^n} dt, \quad (44)$$

and λ again denotes the maximum extent of the worldline in the direction orthogonal to the plates. In the low-temperature limit, $2\xi \ll \sqrt{\langle \lambda^2 \rangle} = \pi/\sqrt{3}$, the exponential integral functions vanish exponentially and can be neglected. We then obtain the small-temperature correction to $E_c^{\parallel}(0)$ in D dimensions fully analytically:

$$\frac{\Delta E_c^{\parallel}(\xi \rightarrow 0)}{E_c^{\parallel}(0)} = \frac{\Gamma\left(\frac{D-1}{2}\right) \sqrt{\pi} \zeta(D-1) (2\xi)^{D-1}}{\Gamma(D/2) \zeta(D)} - (2\xi)^D. \quad (45)$$

The term $(2\xi)^D$ agrees with the standard textbook result [3]. It dominates the thermal correction to the Casimir force, yielding a comparatively suppressed power law dependence on the temperature, $\Delta F_c(T) \sim T^D$ for small T . This is an immediate consequence of the gap in the relevant part of the fluctuation spectrum in this closed geometry. This term can also be understood as an excluded-volume effect: the volume in between the plates cannot be thermally populated by photons at low temperature due to the spectral gap.

Incidentally, the leading contribution to the energy $\sim \xi^{D-1}$ is much less known. It does not contribute to the Casimir force, since it is independent of a when multiplied by the normalization prefactor $E_c^{\parallel}(0)$. As we will see in section IV B, a -independent terms in the energy should not be viewed as mere calculational artefacts but can also contribute to observables such as the Casimir torque. To the best of our knowledge, Eq. (45) represents the first exact analytic formula for this leading small temperature correction to the free energy.

The high-temperature limit of (43) can be obtained by a Poisson resummation of the winding-number sum (which is identical to returning to Matsubara frequency space). Our result agrees with [3] and reads:

$$\frac{\Delta E_c^{\parallel}(\xi \rightarrow \infty)}{E_c^{\parallel}(0)} = -1 + \frac{2\Gamma\left(\frac{D-1}{2}\right) \zeta(D-1) \sqrt{\pi}}{\Gamma(D/2) \zeta(D)} \xi. \quad (46)$$

For arbitrary ξ and $D > 2$, Eq. (43) can be evaluated numerically. Figure 7 shows the worldline result together

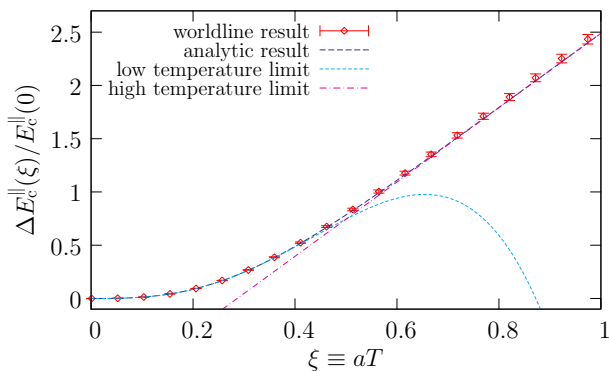


FIG. 7: Parallel plates: temperature dependence of the thermal contribution to the Casimir energy $\Delta E_c^{\parallel}(\xi)/E_c^{\parallel}(0)$ normalized to the zero-temperature result in $D = 4$ -dimensional spacetime versus the dimensionless temperature variable $\xi = aT$. The worldline result for 1000 worldlines with 2×10^6 points each is plotted together with the analytic expressions (45)-(47).

with the analytic asymptotics (45)-(46) and the known exact analytic formula for $D = 4$, see e.g. [46]:

$$\frac{\Delta E_c^{\parallel}(\xi)}{E_c^{\parallel}(0)} = -1 + \frac{90\xi}{\pi^3} \sum_{n=1}^{\infty} \frac{\coth(2n\pi\xi) + 2n\pi\xi \operatorname{csch}^2(2n\pi\xi)}{n^3}. \quad (47)$$

Note that the result obtained in [46] for the electromagnetic field is twice as large as the result for the scalar field (47).

Of course, taking the derivative of (43), (45) or (46) with respect to a also gives immediate access to the thermal corrections $\Delta F_c(T)$ to the Casimir force. For instance, the low-temperature limit results in

$$\begin{aligned} \Delta F_c(aT \ll 1) &= -\frac{\partial}{\partial a} \Delta E_c^{\parallel} \Big|_{aT \ll 1} \\ &= -\frac{\Gamma(D/2)\zeta(D)A}{\pi^{D/2}} T^D, \end{aligned} \quad (48)$$

again revealing the power-law suppressed temperature dependence which is characteristic for a closed geometry. Both magnitude and sign of the thermal force correction can be understood as an excluded-volume effect: as the temperature is small compared to the spectral gap, thermal modes in-between the plates cannot be excited. Hence, the thermal Stefan-Boltzmann energy density outside the plates is not balanced by a thermal contribution inside. Thermal effects therefore enhance the attractive force between the plates.

Let us finally remark that the comparison between the small-temperature limit of (47) (calculated with the help of the Poisson summation) and our analytic formula (45) closes a gap in the literature. With this comparison, we can find the exact value of the integral occurring in the prefactor of the leading low-temperature term in the energy,

$$\int_0^{\infty} dx \frac{1}{2x^4} [-2 + x(\coth x + x \operatorname{csch}^2 x)] = \frac{\zeta(3)}{2\pi^2}, \quad (49)$$

numerically corresponding to ≈ 0.060897 . This result has been observed numerically in the sum over odd reflection contributions to the parallel-plates Casimir energy in the optical approach to the Casimir effect [14].

B. Inclined Plates

Whereas the inclined-plate geometry is much more difficult to deal with than the parallel-plate case when using standard methods, there is comparatively little difference in the worldline language. Inserting the inclined-plates Θ functional (25) with $\gamma_m(x)$ as in Eq. (27) into the general worldline formula (14) yields

$$E_c^{i.p.,\varphi}(\xi) = E_c^{i.p.,\varphi} + \Delta E_c^{i.p.,\varphi}(\xi), \quad (50)$$

where

$$\begin{aligned} \Delta E_c^{i.p.,\varphi}(\xi) &= -\frac{L_y \csc(\varphi)}{(4\pi)^{D/2} a^{D-2}} \left((2\xi)^{D-2} \zeta(D-2) \Gamma\left(\frac{D-2}{2}\right) \left\langle \int_{\gamma_{\min}}^{\gamma_{\max}} dx \gamma_m(x) \right\rangle - \zeta(D-1) (2\xi)^{D-1} \Gamma\left(\frac{D-1}{2}\right) \sqrt{\pi} \right. \\ &\quad \left. + \left\langle \sum_{n=1}^{\infty} \int_{\gamma_{\min}}^{\gamma_{\max}} dx \gamma_m^{D-1}(x) \times \left[E_{\frac{3}{2}-\frac{D}{2}}\left(\frac{\gamma_m^2(x)n^2}{4\xi^2}\right) - E_{2-\frac{D}{2}}\left(\frac{\gamma_m^2(x)n^2}{4\xi^2}\right) \right] \right\rangle \right) \end{aligned} \quad (51)$$

is the thermal contribution to the energy. Here and in the following, we confine ourselves to spacetime dimensions

$D > 3$ where all expressions exhibit well-controlled con-

vergence. In the low-temperature limit, the exponential integral functions can be neglected as long as $\gamma_m(x) \neq 0$ for all x . This is certainly the case for $\varphi \neq 0$, but not necessarily for $\varphi = 0$. The latter case is again identical to the semi-infinite plate parallel to a infinite one, and is being considered separately in the next section and also in the appendix. For $\varphi \neq 0$, the low-temperature limit is then given by the first two terms (first line) of Eq. (51). Note that the first ξ^{D-2} term does not contribute to the Casimir force, since it is an a -independent contribution to E_c if read together with the normalization prefactor. From the second term, we obtain the low-temperature thermal correction to the Casimir force upon differentiation with respect to a ,

$$\Delta F_c^{i.p.,\varphi \neq 0} = -L_y \csc(\varphi) \frac{\Gamma\left(\frac{D-1}{2}\right) \zeta(D-1)}{2\pi^{(D-1)/2}} T^{D-1}. \quad (52)$$

The temperature dependence differs from the parallel-plates case by one power of T , implying a significantly stronger temperature dependence at small temperatures. This is a direct consequence of the fact that we are dealing here with an open geometry. We emphasize that the result has been obtained fully analytically. In $D = 4$ and $\varphi = \pi/2$, our result agrees with the perpendicular-plates study of [15] where this nontrivial interplay between temperature and geometry has been demonstrated for the first time. As shown therein, the thermal correction for this open geometry at experimentally-relevant large separations can be an order of magnitude larger than for a closed geometry.

Whereas the a -independent first term of Eq. (51) does not contribute to the force, both terms in the first line of Eq. (51) contribute to the low-temperature limit of the Casimir torque. The thermal contribution to the torque is

$$\Delta D_c^{i.p.,\varphi}(\xi) = \frac{d\Delta E_c^{i.p.,\varphi}(\xi)}{d\varphi}, \quad (53)$$

which at low temperature reads

$$\begin{aligned} \Delta D_c^{i.p.,\varphi}(\xi \rightarrow 0) &= -\frac{L_y \cos(\varphi)}{(4\pi)^{D/2} \sin^2(\varphi)} \\ &\times \left((2T)^{D-2} \zeta(D-2) \Gamma\left(\frac{D-2}{2}\right) \right. \\ &\quad \times [\langle \gamma_{x_{\min}}(\varphi) \lambda_x \rangle - \tan(\varphi) \langle \gamma'_{x_{\min}}(\varphi) \lambda_x \rangle] \\ &\quad \left. + a \zeta(D-1) (2T)^{D-1} \Gamma\left(\frac{D-1}{2}\right) \sqrt{\pi} \right), \quad (54) \end{aligned}$$

where $\langle \int_{\gamma_{x_{\min}}}^{\gamma_{x_{\max}}} x dx \rangle = 0$ has been used, and we have introduced $\lambda_x = \gamma_{x_{\max}} - \gamma_{x_{\min}}$. This expression depends on only one nontrivial worldline average. In limiting cases, this average can be given analytically, as it reduces to the case described by Eq. (24): we find $-\langle \gamma_{x_{\min}}(\varphi \rightarrow 0) \lambda_x \rangle = \langle \lambda_x^2 \rangle / 2 = \pi^2 / 6$ and $-\langle \gamma'_{x_{\min}}(\varphi \rightarrow \pi/2) \lambda_x \rangle = \langle \lambda_x \rangle^2 / 2 = \pi / 2$. For arbitrary φ , this average

can be well approximated by

$$\langle \gamma_{x_{\min}}(\varphi) \lambda_x \rangle \approx -\frac{\pi}{2} \sin^2(\varphi) - \frac{\pi^2}{6} \cos^2(\varphi), \quad (55)$$

as we will explain in the following. With Eq. (26), we can write

$$\gamma_{x_{\min}}(\varphi) \equiv \gamma_x(\hat{t}) \cos(\varphi) + \gamma_z(\hat{t}) \sin(\varphi), \quad (56)$$

where \hat{t} denotes the value of t that satisfies the minimum condition in Eq. (26). Together with

$$\gamma_{z_{\min}}(\varphi) \equiv -\gamma_x(\hat{t}) \sin(\varphi) + \gamma_z(\hat{t}) \cos(\varphi), \quad (57)$$

we can interpret $(\gamma_{x_{\min}}(\varphi), \gamma_{z_{\min}}(\varphi))$ as the coordinates of the point $(\gamma_x(\hat{t}), \gamma_z(\hat{t}))$ in the φ -rotated system.

Since the γ_x and γ_z coordinates of each loop are generated independently of each other, $\gamma_z(\hat{t})$ and λ_x are not correlated. We therefore obtain

$$\langle \lambda_x \gamma_{x_{\min}}(\varphi) \rangle = \langle \lambda_x \gamma_x(\hat{t}) \rangle \cos(\varphi) + \langle \lambda_x \rangle \langle \gamma_z(\hat{t}) \rangle \sin(\varphi). \quad (58)$$

By symmetry, the average $\langle \gamma_{z_{\min}}(\varphi) \rangle$ vanishes, and we get from Eq. (57)

$$\langle \gamma_x(\hat{t}) \rangle \sin(\varphi) = \langle \gamma_z(\hat{t}) \rangle \cos(\varphi). \quad (59)$$

On the other hand, $\langle \gamma_{x_{\min}}(\varphi) \rangle = -\langle \lambda_x \rangle / 2$. Substituting Eq. (59) into the average of Eq. (56) leads to $\langle \gamma_z(\hat{t}) \rangle = -\sin(\varphi) \langle \lambda_x \rangle / 2$ and $\langle \gamma_x(\hat{t}) \rangle = -\cos(\varphi) \langle \lambda_x \rangle / 2$, such that the desired Eq. (55) can be motivated by Eq. (58). We would like to stress that only the second term in Eq. (55) has been estimated with the constraint imposed by the exactly known result for $\varphi \rightarrow 0$, see above. The first term is exact and dictates the behavior of the perpendicular-plates limit. This result is compared to the numerically obtained data in Fig. 8.

For the v-loop algorithm [24] used here to generate the loops, the expectation value of the maximal extent λ_x is systematically smaller. This error is about the average spacing $(|\gamma_x(t_{i+1}) - \gamma_x(t_i)|) \approx \sqrt{1/2N}$, see Eq. (20). As a consequence, the systematic error of $\langle \lambda_x^2 \rangle / 2$ and $\langle \lambda_x \rangle^2 / 2$ is about $\langle \lambda_x \rangle \sqrt{1/2N} \approx 1.3 \times 10^{-3}$ at $N = 10^6$. We observe a good agreement of the data with Eq.(55) at $\varphi = 0$ and $\varphi = \pi/2$ if the systematic error is taken into account. However, the agreement is actually perfect for all φ when using worldline estimates for the prefactors in Eq. (55) instead of $\pi/2$ and $\pi^2/6$, see the modified curve in Fig. 8. This shows that Eq. (55) will well fit the data in the continuum limit $N \rightarrow \infty$.

Let us return to the calculation of the Casimir torque. In the vicinity of the perpendicular-plates configuration, $\varphi = \pi/2 - \delta\varphi$, we can now obtain an expression to first order in $\delta\varphi$:

$$\begin{aligned} \Delta D_c^{i.p.,\varphi=\pi/2-\delta\varphi}(\xi \rightarrow 0) &= -\frac{L_y \delta\varphi}{(4\pi)^{D/2}} (2T)^{D-2} \\ &\times \left(-\zeta(D-2) \Gamma\left(\frac{D-2}{2}\right) \left[\frac{\pi}{2} - \langle \gamma''_{x_{\min}}\left(\frac{\pi}{2}\right) \lambda_x \rangle \right] \right. \\ &\quad \left. + 2aT \zeta(D-1) \Gamma\left(\frac{D-1}{2}\right) \sqrt{\pi} \right). \quad (60) \end{aligned}$$

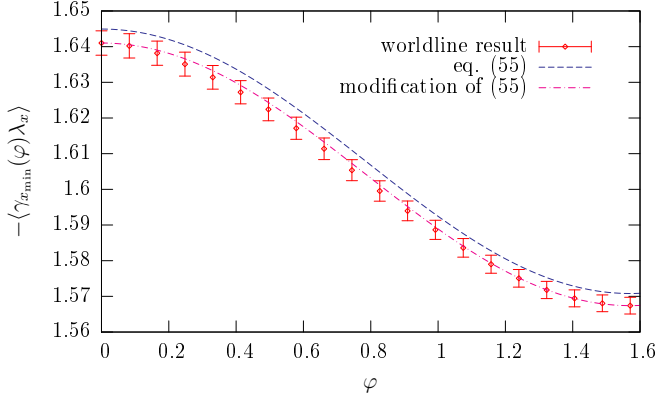


FIG. 8: Angle dependence of the worldline average occurring in the Casimir torque (54): $\langle \gamma_{x_{\min}}(\varphi)\lambda_x \rangle$. The numerical result is compared to the estimate (55) (dashed line). The worldline result shows a small systematic error due to the finite discretization. We can include the systematic error into (55) by taking worldline estimates for the boundary values at $\varphi = 0$ and $\varphi = \pi/2$ (i.e. $1.567 \sin^2(\varphi) + 1.641 \cos^2(\varphi)$), respectively, which are smaller than $\pi/2$ and $\pi^2/6$. This yields the dot-dashed curve. The worldline result has been obtained from $5 \cdot 10^4$ loops with 10^6 ppl each.

Here we have used $\langle \gamma'_{x_{\min}}(\pi/2)\lambda_x \rangle = 0$. Apart from $\langle \gamma''_{x_{\min}}(\pi/2)\lambda_x \rangle$, Eq. (60) is an analytical expression. Using (55), we obtain $-\langle \gamma''_{x_{\min}}(\pi/2)\lambda_x \rangle \approx \pi^2/3 - \pi \approx 0.148$, which is about ten percent of the dominating analytical term in square brackets $\sim \pi/2$. We observe that the first term, which dominates in the limit $aT \rightarrow 0$, gives a contribution to the torque which drives the system away from the perpendicular-plates case $\varphi = \pi/2$. Zero- and finite-temperature contributions thus have the same sign. The fact that $\varphi = \pi/2$ is a repulsive fixed point is also in agreement with naive expectations.

For $D = 4$, Eq. (60) reads

$$\frac{\Delta D_c^{i.p.,\varphi=\pi/2-\delta\varphi}(\xi \rightarrow 0)}{L_y} = \delta\varphi T^2 (0.0716 - 0.0957\xi), \quad (61)$$

which should be compared with the first-order term arising from the $T = 0$ contribution Eq. (37), which reads $D_c^{i.p.,\varphi=\pi/2-\delta\varphi}/L_y \approx 0.00329\delta\varphi/a^2$. Thus, for $D = 4$ we obtain to first order in $\delta\varphi$

$$\frac{\Delta D_c^{i.p.,\varphi=\pi/2-\delta\varphi}(\xi \rightarrow 0)}{D_c^{i.p.,\varphi=\pi/2-\delta\varphi}(0)} \approx \xi^2 (21.8 - 29.1\xi). \quad (62)$$

In the validity regime of the low-temperature expansion, $\xi = aT \ll 1$, the positive first term is always dominant, hence perpendicular-plates case remains a repulsive fixed point. Most importantly, we would like to stress that the quadratic dependence of the torque on the temperature $\sim T^2$ ($\sim T^{D-2}$ in the general case) for the inclined-plates configuration represents the strongest temperature dependence of all observables discussed in this article.

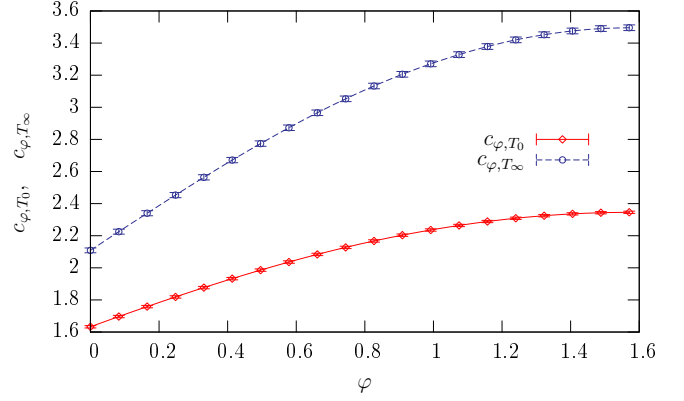


FIG. 9: Integrals appearing in Eqs. (51) and (63) for $D = 4$. We have defined $c_{\varphi,T_0} \equiv \left\langle \int_{\gamma_{x_{\min}}}^{\gamma_{x_{\max}}} dx \gamma_m(x) \right\rangle$ and $c_{\varphi,T_\infty} \equiv \left\langle \int_{\gamma_{x_{\min}}}^{\gamma_{x_{\max}}} dx \gamma_m^2(x) \right\rangle$; see also Eqs. (6), (7) and (9). Employing Eq. (24), we can evaluate $c_{\varphi=0,T_0} = \zeta(2) \approx 1.645$ and $c_{\varphi=0,T_\infty} = \sqrt{\pi}\zeta(3) \approx 2.131$ analytically. We have used 10^4 worldlines with 10^6 ppl each.

The high-temperature limit of Eq. (51) can again be obtained by Poisson summation. The result is:

$$\Delta E_c^{i.p.,\varphi}(\xi \rightarrow \infty) = -E_c^{i.p.,\varphi}(0) - \frac{L_y 2\sqrt{\pi} \left\langle \int_{\gamma_{x_{\min}}}^{\gamma_{x_{\max}}} \gamma_m^{D-2}(x) dx \right\rangle}{(4\pi)^{D/2} a^{D-2} (D-3)(D-2) \sin(\varphi)} \xi. \quad (63)$$

The remaining worldline average in this expression yields some positive finite number. Irrespective of its precise value for a given angle φ and D (the precise value of the integral for a specific φ can be read off, for instance, from Fig. 9 for either $D = 3$ or $D = 4$ and Fig. 4 for $D = 5$), we stress that we observe the same linear dependence on temperature $\xi = aT$ as in the parallel plate case. This is nothing but the familiar phenomenon of the dominance of the zeroth Matsubara mode at high temperatures, implying dimensional reduction, as discussed above. This mechanism is obviously geometry independent. Also the Casimir force remains attractive also for high temperatures.

C. Semi-infinite plate parallel to an infinite plate

A particularly interesting example for the geometry-temperature interplay is given by the semi-infinite plate parallel to the infinite plate (1si configuration). In this case, the angle of inclination φ in Fig. 29 is zero. Analogously to Eq. (29), the finite-temperature Casimir energy can be decomposed as

$$E_c^{1si}(\xi) = E_c^{1si,edge}(\xi) + E_c^{1si,\parallel}(\xi), \quad (64)$$

where $E_c^{1\text{si},\parallel}(T) = E_c^{1\text{si},\parallel}(0) + \Delta E_c^{1\text{si},\parallel}(T)$ correspond to the standard parallel-plate formulas as given in Eqs. (23) and (43), with A being now the surface of the semi-infinite plate. Approaching the 1si limit of $\Delta E_c^{1\text{si},\parallel}(T)$ from the inclined-plates configuration in the limit $\varphi \rightarrow 0$ is again a delicate issue, as the proper order of limits $\varphi \rightarrow 0$ and $L_z \rightarrow \infty$ has to be accounted for, see

$$\Delta E_c^{1\text{si},\text{edge}}(\xi) = -\frac{L_y}{(4\pi)^{D/2} a^{D-2}} \left[(2\xi)^{D-2} \zeta(D-2) \Gamma\left(\frac{D-2}{2}\right) \left\langle \int_{\gamma_{x_{\min}}}^{\gamma_{x_{\max}}} dx \gamma_{z_{\max}}(x) \right\rangle - \sum_{n=1}^{\infty} \left\langle \int_{\gamma_{x_{\min}}}^{\gamma_{x_{\max}}} dx (x - \gamma_{x_{\min}})^{D-2} \gamma_{z_{\max}}(x) E_{2-\frac{D}{2}}\left(\frac{(x - \gamma_{x_{\min}})^2 n^2}{4\xi^2}\right) \right\rangle \right]. \quad (65)$$

Note that the first term, being the main contribution to the Casimir energy at small T , does not contribute to the Casimir force since it is a independent. Contrary to the case with $\varphi \neq 0$, the exponential integral functions cannot be neglected in the low-temperature limit, since the argument of $E_n(z)$ becomes zero at the lower bound of the integral for any $\xi > 0$. This results in a correction $\sim \xi^{D-1+\alpha}$, with $\alpha > 0$, to the low-temperature limit of the first term.

Here, however, we concentrate on the last term, as it gives rise to the thermal correction of the Casimir force. In the low-temperature limit, we find

$$-\Delta F_c^{1\text{si},\text{edge}}(\xi) = \frac{2L_y}{(4\pi)^{D/2} a^{D-1}} \sum_{n=1}^{\infty} \left\langle \int_0^{\lambda_x} dx x^{D-2} \gamma_{z_{\max}}(\gamma_{x_{\min}} + x) \exp\left(-\frac{x^2 n^2}{4\xi^2}\right) \right\rangle. \quad (66)$$

For small ξ , the main contribution to the integral comes from its lower bound as the exponential function rapidly decreases for large argument. At the lower bound, we can take the worldline average $\langle \gamma_{z_{\max}}(\gamma_{x_{\min}} + x) \rangle$ first, yielding a smooth function. We expand the latter in a power series,

$$\langle \gamma_{z_{\max}}(\gamma_{x_{\min}} + x) \rangle = \sum_{n=0}^{\infty} c_n x^{\alpha_n}, \quad (67)$$

where the exponents α_n do not necessarily have to be integers. Inserting (67) into (66) leads to

$$-\Delta F_c^{1\text{si},\text{edge}}(\xi \rightarrow 0) = \frac{L_y}{(4\pi)^{D/2} a^{D-1}} \times \sum_{n=0}^{\infty} c_n (2\xi)^{D+\alpha_n-1} \Gamma\left(\frac{D+\alpha_n-1}{2}\right) \zeta(D+\alpha_n-1), \quad (68)$$

where we have neglected exponentially suppressed contributions. For the lowest-order term, we obtain

Sect. III C. As the analysis is technically involved (but the outcome obvious), we defer it to the appendix. Let us here concentrate on the temperature-dependent edge contribution $\Delta E_c^{1\text{si},\text{edge}}(T) = E_c^{1\text{si},\text{edge}}(T) - E_c^{1\text{si},\text{edge}}(0)$. We set $\varphi = 0$ in Eq. (25) and evaluate Eq. (14). The result is (here and in the following, we confine ourselves to $D > 3$):

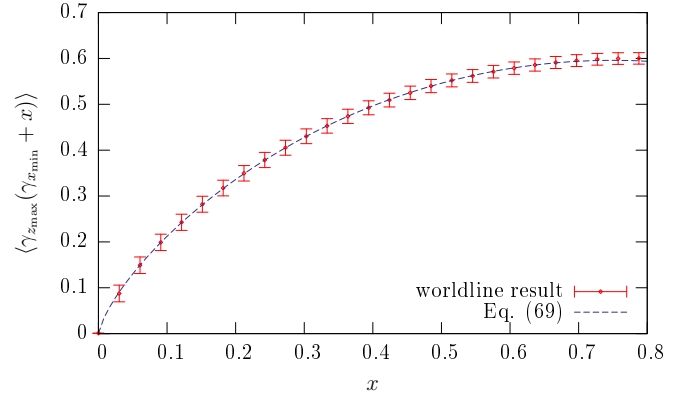


FIG. 10: Numerical result of the worldline average $\langle \gamma_{z_{\max}}(\gamma_{x_{\min}} + x) \rangle$ obtained by $5 \cdot 10^4$ worldlines with 10^6 points each compared to the fit function of Eq. (69) obtained on the interval $x = [0, 0.7]$. The error bars have been plotted ten times larger. The observed small- x power law x^{α_1} with $\alpha_1 \simeq 0.74$ directly translates into a non-integer small-temperature behavior of the thermal edge contribution to the force, $\Delta F_c^{1\text{si},\text{edge}} \sim T^{D-1+\alpha_1}$.

$\langle \gamma_{z_{\max}}(\gamma_{x_{\min}}) \rangle \equiv c_0 = 0$, since for a given worldline $(\gamma_x(t), \gamma_z(t))$ there exists a corresponding worldline in the ensemble with $(\gamma_x(t), -\gamma_z(t))$. We conclude that the coefficient of the T^{D-1} term vanishes. We determine the higher coefficients c_n from computing $\langle \gamma_{z_{\max}}(\gamma_{x_{\min}} + x) \rangle$ in the vicinity of $x = 0$ by worldline numerics. Figure 10 depicts the form of $\langle \gamma_{z_{\max}}(\gamma_{x_{\min}} + x) \rangle$ near the lower bound $x = 0$. A global fit to this function including two coefficients c_1, c_2 is given by

$$\langle \gamma_{z_{\max}}(\gamma_{x_{\min}} + x) \rangle \approx 0.9132 (x(1.500 - x))^{0.7423} \approx 1.234x^{0.7423} - 0.6106x^{1.7423}, \quad (69)$$

where we have kept $\alpha_2 - \alpha_1 = 1$ fixed. The resulting thermal correction to the force is shown in Fig. (11)

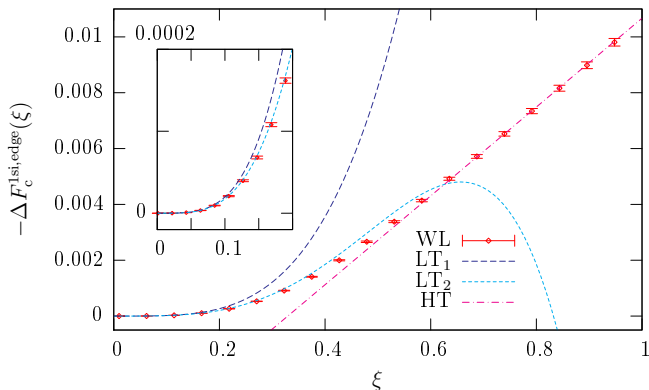


FIG. 11: Thermal contribution to the Casimir edge force in the 1si configuration, $-\Delta F_c^{1si,edge}(\xi)$, plotted for $a = 1$ and $D = 4$. WL: worldline result Eq. (66) obtained using 1000 loops with 10^6 ppl each. LT_1 , LT_2 : leading and next-to-leading low-temperature corrections $0.1098\xi^{3.7423}$ and $0.1098\xi^{3.7423} - 0.131881\xi^{4.7423}$, respectively, obtained from Eqs. (68) and (69), using 5×10^4 loops 10^6 ppl each. HT: high temperature limit obtained from Eq. (70), using 5×10^4 loops 10^6 ppl each; a fit to the HT curve is provided by $-5.24062(\pm 0.0222)10^{-3} + 1.591(\pm 0.004138)10^{-2}\xi$. The inlay displays a magnified interval $\xi = [0, 0.2]$.

for $D = 4$, where we compare the full numerical solution with different orders of the expansion (69) and the high-temperature asymptotics, see below. As the low-temperature asymptotics is directly related to the lowest nonvanishing coefficient α_1 , we have also performed local fits to the function $\langle \gamma_{z_{\max}}(\gamma_{x_{\min}} + x) \rangle$ in the vicinity of $x = 0$. Depending on the fit window, the leading exponent can grow up to $\alpha_1 \approx 0.8$. (Of course, the fit window must be large enough to avoid that the worldline discretization becomes visible; otherwise, the exponent trivially but artificially approaches $\alpha_1 \rightarrow 1$ as the discretized worldline is a polygon on a microscopic scale).

In any case, we conclude that the low-temperature regime of the 1si edge effect is well described by a non-integer power law, $\Delta F_c^{1si,edge} \sim T^{D-1+\alpha_1} \simeq T^{D-0.3}$, where the fractional exponent arises from the geometry-temperature interplay in this open geometry. Of course, our numerical analysis cannot guarantee to yield the true asymptotic behavior in the limit $\xi \rightarrow 0$, but our data in the low-temperature domain $0.01 \lesssim \xi \lesssim 0.4$ is well described by the non-integer scaling at next-to-leading order.

Let us finally turn to the high-temperature limit of Eq. (65) which can again be obtained by Poisson summation. The result for the edge energy reads

$$\Delta E_c^{1si,edge}(\xi \rightarrow \infty) = -E_c^{1si,edge}(0) \quad (70)$$

$$= -\frac{2\sqrt{\pi}L_y \left\langle \int_0^{\lambda x} dx x^{D-3} \gamma_{z_{\max}}(x + \gamma_{x_{\min}}) \right\rangle}{(4\pi)^{D/2} a^{D-2} (D-3)} \xi,$$

where the worldline average is subject to numerical evaluation. The resulting high-temperature limit of the Casimir force is shown in Fig. (70) for $D = 4$. The high-temperature limit is again linear in T in accordance with general dimensional-reduction arguments.

V. CONCLUSIONS

In this work, we have provided further numerical as well as analytical evidence for the nontrivial interplay between geometry and temperature in the Casimir effect. Whereas closed geometries such as the parallel-plates case exhibit a comparatively strong suppression of thermal corrections at low temperatures, open geometries such as the general inclined-plates geometry reveal a more pronounced temperature dependence in this regime. The terminology *open* and *closed* corresponds to the absence or presence of a gap in the relevant part of the spectrum of fluctuations which gives rise to the Casimir effect. In closed geometries, the spectral gap inhibits sizable fluctuations at temperatures below the scale set by the gap. By contrast, open geometries allow for sizable thermal fluctuations at any value of the temperature.

Concentrating on the inclined-plates geometry in D dimensions, the temperature dependence of the Casimir force can become stronger by one power in the temperature parameter (implying thermal corrections which can be an order of magnitude larger than for a closed geometry). The inclined-plates geometry is particularly interesting as the limit of a semi-infinite plate parallel to an infinite plate (1si configuration) is somewhat in-between open and closed geometries: the open part of the spectrum only arises due to the edge of the semi-infinite plate. Interestingly, the resulting thermal correction numerically shows a power-law temperature dependence with a non-integer exponent $\sim T^{D-0.3}$.

The strongest temperature dependence $\sim T^{D-2}$ in the low-temperature limit occurs for the Casimir torque of the inclined-plates configuration. This is, because it arises from the leading thermal correction of the interaction energy which contributes to the torque but not to the Casimir force.

Our results have been derived for the case of a fluctuating scalar field obeying Dirichlet boundary conditions on the surfaces. Whereas this model system should not be considered as a quantitatively appropriate model for the real electromagnetic Casimir effect, our general conclusions about the geometry-temperature interplay are not restricted to the Dirichlet scalar case. On the contrary, all our arguments based on the presence or absence of a spectral gap will also be valid for the electromagnetic case. Whether or not the case of Neumann or electromagnetic boundary conditions leads to different power-law exponents for the temperature dependence of the “geothermal” phenomena remains an interesting question for future research.

In view of the fact that most (strictly speaking all)

experiments are performed in open geometries, e.g., the sphere-plate geometry, at room temperature, an analysis of the geometry-temperature interplay of these experimentally relevant configurations is most pressing.

same limit for the thermal correction to the energy. The decomposition of the 1si Casimir energy into bulk and edge contributions can also be performed for the thermal corrections,

APPENDIX A: INCLINED PLATES, $\varphi \rightarrow 0$ LIMIT AT FINITE TEMPERATURE

We have analyzed the $\varphi \rightarrow 0$ behavior of inclined plates at zero temperature in Sect. III C. Here, we consider the

$$\Delta E_c^{1\text{si},\varphi}(\xi) = \Delta E_c^{\text{edge},\varphi}(\xi) + \Delta E_c^{\parallel,\varphi}(\xi),$$

where

$$\begin{aligned} \Delta E_c^{\parallel,\varphi}(\xi) = & -\frac{L_y \csc(\varphi)}{(4\pi)^{D/2} a^{D-2}} \left\langle \left[-\Gamma\left(\frac{D-2}{2}\right) \zeta(D-2)(2\xi)^{D-2} \lambda_x \gamma_{x_{\min}}(\varphi) - \zeta(D-1) \Gamma\left(\frac{D-1}{2}\right) (2\xi)^{D-1} \sqrt{\pi} \right. \right. \\ & \left. \left. - \sum_{n=1}^{\infty} \int_{\gamma_{x_{\min}}}^{\gamma_{x_{\max}}} dx \left\{ \gamma_m^{D-2}(x) E_{2-\frac{D}{2}}\left(\frac{n^2 \gamma_m^2(x)}{4\xi^2}\right) (x \cos(\varphi) - \gamma_{x_{\min}}(\varphi)) - \gamma_m^{D-1}(x) E_{\frac{3-D}{2}}\left(\frac{n^2 \gamma_m^2(x)}{4\xi^2}\right) \right\} \right] \right\rangle, \end{aligned} \quad (\text{A1})$$

with $\gamma_m(x) = x \cos(\varphi) + \sin(\varphi) \gamma_{z_{\max}}(x) - \gamma_{x_{\min}}(\varphi)$ and

$$\begin{aligned} \Delta E_c^{\text{edge},\varphi}(\xi) = & -\frac{L_y}{(4\pi)^{D/2} a^{D-2}} \left[\Gamma\left(\frac{D-2}{2}\right) \zeta(D-2)(2\xi)^{D-2} \left\langle \int_{\gamma_{x_{\min}}}^{\gamma_{x_{\max}}} dx \gamma_{z_{\max}}(x) \right\rangle \right. \\ & \left. - \sum_{n=1}^{\infty} \left\langle \int_{\gamma_{x_{\min}}}^{\gamma_{x_{\max}}} dx \gamma_m^{D-2}(x) E_{2-\frac{D}{2}}\left(\frac{n^2 \gamma_m^2(x)}{4\xi^2}\right) \gamma_{z_{\max}}(x) \right\rangle \right]. \end{aligned} \quad (\text{A2})$$

Whereas $\Delta E_c^{\text{edge},\varphi}(\xi)$ remains finite, $\Delta E_c^{\parallel,\varphi}(\xi)$ shows a divergent behavior as $\varphi \rightarrow 0$. Let us therefore concentrate on $\Delta E_c^{\parallel,\varphi}(\xi)$, in order to isolate the source of the apparent divergence which is related to the order of limits of $L_z \rightarrow \infty$ and $\varphi \rightarrow 0$. In the case of inclined plates, $(L_z \varphi)$ is infinite for all $\varphi \neq 0$, resulting in a $1/\varphi$ divergent energy density (energy per length) for $\varphi \rightarrow 0$. Parallel plates, on the other hand have a finite energy density

(energy per area) and $(L_z \varphi) = 0$.

In the following, we show how to obtain an analytic transition from $(L_z \varphi) \rightarrow \infty$ to $(L_z \varphi) \rightarrow 0$ for small φ by working with large but finite L_z , and taking $L_z \rightarrow \infty$ at the end of the calculation. The first limit results in a divergent energy density per unit edge length of the inclined plates as $\varphi \rightarrow 0$,

$$\begin{aligned} \Delta E_c^{\parallel,\varphi \rightarrow 0}(\xi) = & -\frac{L_y}{2a^{D-2} \varphi (4\pi)^{D/2}} \left[\langle \lambda^2 \rangle \Gamma\left(\frac{D-2}{2}\right) \zeta(D-2)(2\xi)^{D-2} - 2(2\xi)^{D-1} \zeta(D-1) \Gamma\left(\frac{D-1}{2}\right) \sqrt{\pi} \right. \\ & \left. + \Gamma\left(\frac{D}{2}\right) \zeta(D)(2\xi)^D - \left\langle \lambda^D \sum_{n=1}^{\infty} \left(E_{1-\frac{D}{2}}\left(\frac{\lambda^2 n^2}{4\xi^2}\right) + E_{2-\frac{D}{2}}\left(\frac{\lambda^2 n^2}{4\xi^2}\right) - 2E_{\frac{3}{2}-\frac{D}{2}}\left(\frac{\lambda^2 n^2}{4\xi^2}\right) \right) \right\rangle \right] + \mathcal{O}(1). \end{aligned} \quad (\text{A3})$$

The second limit corresponds to the finite energy density of exact parallel plates (43).

In Eqs. (A1-A3), the z integration was performed first. Let us now do the proper time integration first. The θ function (33), valid for small φ , reflects itself in the lower

end of the proper time integral:

$$\begin{aligned} \Delta E_c^{\parallel,\varphi \rightarrow 0}(a, \beta) = & -\frac{L_y}{(4\pi)^{D/2}} \left\langle \sum_{n=1}^{\infty} \right. \\ & \times \int_1^{\infty} \frac{\exp\left(-\frac{\beta^2 x^2 n^2}{4T(a+z\varphi)^2}\right) d\mathcal{T}}{\mathcal{T}^{\frac{D+1}{2}}} \\ & \left. \times \int_0^{L_z/2} \frac{dz}{(a+z\varphi)^{D-1}} \int_0^{\lambda_x} x^{D-1} dx \right\rangle. \end{aligned} \quad (\text{A4})$$

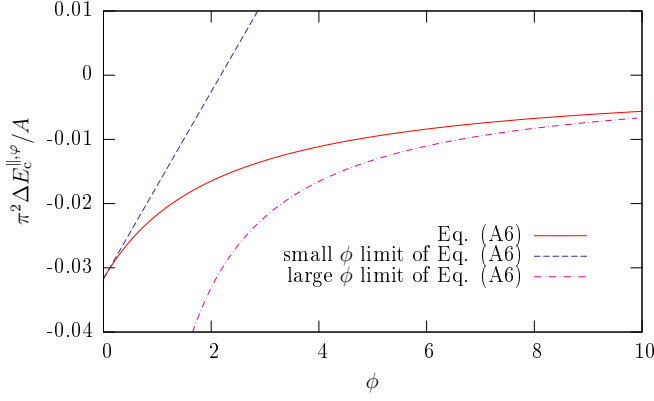


FIG. 12: Qualitative behavior of the thermal Casimir contribution of the bulk in the inclined-plates case Eq. (A7) (red line) and its small- ϕ (dashed blue line) and large- ϕ (dot-dashed magenta line) limit, respectively. Note the divergent $1/\phi$ behavior of the large- ϕ limit which corresponds to the divergent (as $\varphi \rightarrow 0$) energy per edge length in the inclined-plates formulas. For this illustration, we have chosen $D = 4$, $a = \beta = \lambda_x = 1$, ignoring the worldline average in Eq. (A7) for simplicity.

The proper time integration yields for $\text{Re}[D] > 1$:

$$\int_1^\infty \frac{\exp\left(-\frac{\beta^2 x^2 n^2}{4\mathcal{T}(a+z\varphi)^2}\right) d\mathcal{T}}{\mathcal{T}^{\frac{D+1}{2}}} = \left(\frac{2(a+z\varphi)}{xn\beta}\right)^{D-1} \Gamma\left(\frac{D-1}{2}\right) - E_{\frac{3-D}{2}}\left(\frac{x^2\beta^2 n^2}{4(a+z\varphi)^2}\right). \quad (\text{A5})$$

Inserting Eq. (A5) into Eq. (A4) leads to

$$\begin{aligned} \frac{\pi^{\frac{D}{2}} \Delta E_c^{\parallel, \varphi \rightarrow 0}(a, \beta)}{A} &= \sum_{n=1}^{\infty} \left\langle \frac{a^2 \left(\Gamma\left(\frac{D}{2}, \frac{\lambda_x^2 n^2 \beta^2}{4a^2}\right) - \Gamma\left(\frac{D}{2}, \frac{\lambda_x^2 n^2 \beta^2}{(2a+\phi)^2}\right) \right)}{\phi(n\beta)^D} + \frac{\lambda_x^2 \left(\Gamma\left(\frac{D-2}{2}, \frac{\lambda_x^2 n^2 \beta^2}{4a^2}\right) - \Gamma\left(\frac{D-2}{2}, \frac{\lambda_x^2 n^2 \beta^2}{(2a+\phi)^2}\right) \right)}{4\phi(n\beta)^{D-2}} \right. \\ &\quad - \frac{a\lambda_x \left(\Gamma\left(\frac{D-1}{2}, \frac{\lambda_x^2 n^2 \beta^2}{4a^2}\right) - \Gamma\left(\frac{D-1}{2}, \frac{\lambda_x^2 n^2 \beta^2}{(2a+\phi)^2}\right) \right)}{\phi(n\beta)^{D-1}} + \frac{\phi \left(\Gamma\left(\frac{D}{2}\right) - \Gamma\left(\frac{D}{2}, \frac{\lambda_x^2 n^2 \beta^2}{(2a+\phi)^2}\right) \right)}{4(n\beta)^D} \\ &\quad \left. + \frac{\lambda_x \Gamma\left(\frac{D-1}{2}, \frac{\lambda_x^2 n^2 \beta^2}{(2a+\phi)^2}\right)}{2(n\beta)^{D-1}} - \frac{a\Gamma\left(\frac{D}{2}, \frac{L^2 n^2 \beta^2}{(2a+\phi)^2}\right)}{(n\beta)^D} \right\rangle - \frac{\sqrt{\pi}\Gamma\left(\frac{D-1}{2}\right)\zeta(D-1)}{2\beta^{D-1}} + \frac{a\Gamma\left(\frac{D}{2}\right)\zeta(D)}{\beta^D}, \quad (\text{A6}) \end{aligned}$$

where $\phi \equiv L_z \varphi$ and $A = L_y L_z / 2$. One can show that the first three terms of Eq. (A6) are of order $\mathcal{O}(\phi^2)$. The fourth term is clearly $\mathcal{O}(\phi)$. The last line can be converted into the parallel-plates energy density (43) by neglecting ϕ with respect to a and using the identity $z^\alpha E_{1-\alpha}(z) = \Gamma(\alpha, z)$; the error is of order $\mathcal{O}(\phi^2)$. The first-order correction to the parallel-plates case is there-

fore encoded in the fourth term. The second-order correction is in the first three terms since the ϕ^2 terms cancel each other in the remainder. In this limit ($|\phi| \ll 1$), all sums converge for $\text{Re}[D] > 2$.

Let us rearrange (A6) so as to investigate the $\phi \rightarrow \infty$ case with φ being small but finite:

$$\begin{aligned} \frac{\pi^{\frac{D}{2}} \Delta E_c^{\parallel, \varphi}(a, \beta)}{A} = & \sum_{n=1}^{\infty} \left\langle \frac{(4a + \phi) \left(\Gamma\left(\frac{D}{2}\right) - \Gamma\left(\frac{D}{2}, \frac{\lambda_x^2 n^2 \beta^2}{(2a + \phi)^2}\right) \right)}{4(n\beta)^D} + \frac{\lambda_x \left(\Gamma\left(\frac{D-1}{2}, \frac{\lambda_x^2 n^2 \beta^2}{(2a + \phi)^2}\right) - \Gamma\left(\frac{D-1}{2}\right) \right)}{2(n\beta)^{D-1}} \right. \\ & - \frac{\lambda_x^2 \Gamma\left(\frac{D-2}{2}, \frac{\lambda_x^2 n^2 \beta^2}{(2a + \phi)^2}\right)}{4\phi(n\beta)^{D-2}} + \frac{a\lambda_x \Gamma\left(\frac{D-1}{2}, \frac{\lambda_x^2 n^2 \beta^2}{(2a + \phi)^2}\right)}{\phi(n\beta)^{D-1}} - \frac{a^2 \Gamma\left(\frac{D}{2}, \frac{\lambda_x^2 n^2 \beta^2}{(2a + \phi)^2}\right)}{\phi(n\beta)^D} \\ & \left. + \frac{\lambda_x^2 \Gamma\left(\frac{D-2}{2}, \frac{\lambda_x^2 n^2 \beta^2}{4a^2}\right)}{4\phi(n\beta)^{D-2}} - \frac{a\lambda_x \Gamma\left(\frac{D-1}{2}, \frac{\lambda_x^2 n^2 \beta^2}{4a^2}\right)}{\phi(n\beta)^{D-1}} + \frac{a^2 \Gamma\left(\frac{D}{2}, \frac{\lambda_x^2 n^2 \beta^2}{4a^2}\right)}{\phi(n\beta)^D} \right\rangle. \end{aligned} \quad (\text{A7})$$

The large- ϕ behavior of the first two terms can be obtained through Poisson summation³ and reads

$$\frac{(4a + \phi)(c_1 + c_2(2a + \phi))}{(2a + \phi)^D} + \frac{(c_3 + c_4(2a + \phi))}{(2a + \phi)^{D-1}}, \quad (\text{A8})$$

where c_1, \dots, c_4 are constants, the values of which are of no importance. We see that Eq. (A8) vanishes for $D > 2$. For $D > 3$ the terms vanish even if multiplied

by the infinite length L_z . Remember that the inclined-plates formulae at finite temperature are valid for $D > 3$ as well.

In order to keep the remaining terms of Eq. (A7) finite, we multiply both sides with the infinite length L_z converting the vanishing Casimir energy per area into the finite energy per length. The Poisson summation of the second line of Eq. (A7) results in

$$\begin{aligned} \lim_{\phi \rightarrow \infty} \sum_{n=1}^{\infty} \left(-\frac{\lambda_x^2 \Gamma\left(\frac{D-2}{2}, \frac{\lambda_x^2 n^2 \beta^2}{(2a + \phi)^2}\right)}{4\phi(n\beta)^{D-2}} + \frac{a\lambda_x \Gamma\left(\frac{D-1}{2}, \frac{\lambda_x^2 n^2 \beta^2}{(2a + \phi)^2}\right)}{\phi(n\beta)^{D-1}} - \frac{a^2 \Gamma\left(\frac{D}{2}, \frac{\lambda_x^2 n^2 \beta^2}{(2a + \phi)^2}\right)}{\phi(n\beta)^D} \right) = & -\frac{\lambda_x^2 \Gamma\left(\frac{D-2}{2}\right) \zeta(D-2)}{4\phi\beta^{D-2}} \\ & + \frac{a\lambda_x \Gamma\left(\frac{D-1}{2}\right) \zeta(D-1)}{\phi\beta^{D-1}} - \frac{a^2 \Gamma\left(\frac{D}{2}\right) \zeta(D)}{\phi\beta^D} + \frac{d_1 + d_2(2a + \phi)}{\phi(2a + \phi)^{D-2}} + \frac{d_3 + d_4(2a + \phi)}{\phi(2a + \phi)^{D-1}} + \frac{d_5 + d_6(2a + \phi)}{\phi(2a + \phi)^D}, \end{aligned} \quad (\text{A9})$$

where d_1, \dots, d_6 are constants. These terms containing d_i 's vanish for $D > 3$ and $\phi \rightarrow \infty$. Applying the identity $z^a E_{1-a}(z) = \Gamma(a, z)$ to the last three terms in Eq. (A7), we rediscover the inclined-plates formula (A3) from Eqs. (A7), (A9) valid for small angles φ . From Eqs. (A8) and (A9), one can infer that the first correction to Eq. (A3) is of order $O(1/\phi^{D-3})$.

ACKNOWLEDGMENTS

The authors are grateful to Klaus Klingmüller for interesting discussions. AW acknowledges support by

the Landesgraduiertenförderung Baden-Württemberg, by the Heidelberg Graduate School of Fundamental Physics, and by the DFG under contract Gi 328/3-2. HG was supported by the DFG under contract No. Gi 328/1-4 (Emmy-Noether program), Gi 328/5-1 (Heisenberg program).

- [1] H.B.G. Casimir, Kon. Ned. Akad. Wetensch. Proc. **51**, 793 (1948).
 [2] M. Bordag, U. Mohideen and V. M. Mostepanenko, Phys. Rept. **353**, 1 (2001); R. Onofrio, New J. Phys. **8**, 237 (2006) [arXiv:hep-ph/0612234]; S. Y. Buhmann and D. G. Welsch, Prog. Quant. Electron. **31**, 51 (2007) [arXiv:quant-ph/0608118].

- [3] K. A. Milton, "The Casimir effect: Physical manifestations of zero-point energy," *River Edge, USA: World Scientific (2001)*.
 [4] S. K. Lamoreaux, Phys. Rev. Lett. **78**, 5 (1997); U. Mohideen and A. Roy, Phys. Rev. Lett. **81**, 4549 (1998); H.B. Chan *et al.*, Science **291**, 1941 (2001); R.S. Decca *et al.*, Phys. Rev. D **68**, 116003 (2003); Phys. Rev. Lett.

- 94**, 240401 (2005).
- [5] M. Boström and Bo E. Sernelius, *Phys. Rev. Lett.* **84**, 4757 (2000).
- [6] V. M. Mostepanenko *et al.*, *J. Phys. A* **39**, 6589 (2006) [arXiv:quant-ph/0512134].
- [7] I. Brevik, S. A. Ellingsen and K. A. Milton, arXiv:quant-ph/0605005.
- [8] G. Bimonte, *Phys. Rev. A* **79**, 042107 (2009) [arXiv:0903.0951 [quant-ph]].
- [9] G.-L. Ingold, A. Lambrecht, S. Reynaud, arXiv:0905.3608 [quant-ph] (2009).
- [10] C.C. Speake and C. Trenkel, *Phys. Rev. Lett.* **90**, 160403 (2003).
- [11] W.J. Kim, M. Brown-Hayes, D.A.R. Dalvit, J.H. Brownell, R. Onofrio, *Phys. Rev. A* **78**, 020101(R) (2008) [arXiv:0812.0028v1 [quant-ph]].
- [12] R. S. Decca, E. Fischbach, G. L. Klimchitskaya, D. E. Krause, D. López, U. Mohideen, V. M. Mostepanenko, *Phys. Rev. A* **79**, 026101 (2009), [arXiv:0809.3576 [quant-ph]].
- [13] W.J. Kim, M. Brown-Hayes, D.A.R. Dalvit, J.H. Brownell, R. Onofrio, *Phys. Rev. A* **79**, 026102 (2009) [arXiv:0903.1085 [quant-ph]].
- [14] A. Scardicchio and R. L. Jaffe, *Nucl. Phys. B* **743** (2006) 249 [arXiv:quant-ph/0507042].
- [15] H. Gies and K. Klingmuller, *J. Phys. A* **41**, 164042 (2008).
- [16] H. Gies and K. Klingmuller, *Phys. Rev. Lett.* **97**, 220405 (2006) [arXiv:quant-ph/0606235].
- [17] H. Gies, K. Langfeld and L. Moyaerts, *JHEP* **0306**, 018 (2003); arXiv:hep-th/0311168.
- [18] R.P. Feynman, *Phys. Rev.* **80**, 440 (1950); **84**, 108 (1951).
- [19] M. B. Halpern and W. Siegel, *Phys. Rev. D* **16**, 2486 (1977); A. M. Polyakov, "Gauge Fields And Strings," Harwood, Chur (1987) Z. Bern and D.A. Kosower, *Nucl. Phys.* **B362**, 389 (1991); **B379**, 451 (1992) M.J. Strassler, *Nucl. Phys.* **B385**, 145 (1992).
- [20] M. G. Schmidt and C. Schubert, *Phys. Lett. B* **318**, 438 (1993) [arXiv:hep-th/9309055]; for a review, see C. Schubert, *Phys. Rept.* **355**, 73 (2001).
- [21] H. Gies and K. Langfeld, *Nucl. Phys. B* **613**, 353 (2001); *Int. J. Mod. Phys. A* **17**, 966 (2002).
- [22] H. Gies and K. Klingmuller, *J. Phys. A* **39** 6415 (2006) [arXiv:hep-th/0511092].
- [23] H. Gies and K. Klingmuller, *Phys. Rev. Lett.* **96**, 220401 (2006) [arXiv:quant-ph/0601094].
- [24] H. Gies and K. Klingmuller, *Phys. Rev. D* **74**, 045002 (2006) [arXiv:quant-ph/0605141].
- [25] M. Schaden, *Phys. Rev. Lett.* **102**, 060402 (2009).
- [26] B.V. Derjaguin, I.I. Abrikosova, E.M. Lifshitz, *Q.Rev.* **10**, 295 (1956); J. Blocki, J. Randrup, W.J. Swiatecki, C.F. Tsang, *Ann. Phys. (N.Y.)* **105**, 427 (1977).
- [27] M. Schaden and L. Spruch, *Phys. Rev. A* **58**, 935 (1998); *Phys. Rev. Lett.* **84** 459 (2000)
- [28] A. Scardicchio and R. L. Jaffe, *Nucl. Phys. B* **704**, 552 (2005); *Phys. Rev. Lett.* **92**, 070402 (2004).
- [29] R. Balian and B. Duplantier, *Annals Phys.* **112**, 165 (1978).
- [30] A. Bulgac, P. Magierski and A. Wirzba, *Phys. Rev. D* **73**, 025007 (2006) [arXiv:hep-th/0511056]; A. Wirzba, A. Bulgac and P. Magierski, *J. Phys. A* **39** (2006) 6815 [arXiv:quant-ph/0511057].
- [31] T. Emig, R. L. Jaffe, M. Kardar and A. Scardicchio, *Phys. Rev. Lett.* **96** (2006) 080403.
- [32] M. Bordag, *Phys. Rev. D* **73**, 125018 (2006); *Phys. Rev. D* **75**, 065003 (2007).
- [33] O. Kenneth and I. Klich, *Phys. Rev. Lett.* **97**, 160401 (2006); arXiv:0707.4017.
- [34] T. Emig, N. Graham, R. L. Jaffe and M. Kardar, arXiv:0707.1862; arXiv:0710.3084.
- [35] R. B. Rodrigues, P. A. Maia Neto, A. Lambrecht and S. Reynaud, *Phys. Rev. Lett.* **96**, 100402 (2006) [arXiv:quant-ph/0603120]; *Phys. Rev. A* **75**, 062108 (2007).
- [36] F. D. Mazzitelli, D. A. R. Dalvit and F. C. Lombardo, *New J. Phys.* **8**, 240 (2006); D. A. R. Dalvit, F. C. Lombardo, F. D. Mazzitelli and R. Onofrio, *Phys. Rev. A* **74**, 020101 (2006).
- [37] K. A. Milton and J. Wagner, *Phys. Rev. D* **77**, 045005 (2008) [arXiv:0711.0774 [hep-th]]; *J. Phys. A* **41**, 155402 (2008) [arXiv:0712.3811 [hep-th]].
- [38] K. A. Milton, P. Parashar and J. Wagner, arXiv:0806.2880 [hep-th].
- [39] M. Bordag, D. Robaschik and E. Wieczorek, *Annals Phys.* **165**, 192 (1985).
- [40] T. Emig, A. Hanke and M. Kardar, *Phys. Rev. Lett.* **87** (2001) 260402.
- [41] T. Emig and R. Buscher, *Nucl. Phys. B* **696**, 468 (2004).
- [42] H. Gies, J. Sanchez-Guillen and R. A. Vazquez, *JHEP* **0508**, 067 (2005) [arXiv:hep-th/0505275].
- [43] H. Vershelde, L. Wille and P. Phariseau, *Phys. Lett. B* **149**, (1984) .
- [44] N. F. Svaiter and B. F. Svaiter, *J. Math. Phys.* **32** , 175 (1991) .
- [45] K. Klingmuller, Dissertation, Heidelberg U. (2007).
- [46] J. Feinberg, A. Mann and M. Revzen, *Annals Phys.* **288** (2001) 103 [arXiv:hep-th/9908149].